Epigenetic delineation of the earliest cardiac lineage segregation by single-cell multi-omics

Peng Xie[1,2,10], Xu Jiang[3,10], Jingjing He[3,10], Qingyun Pan[3,10], Xianfa Yang [4,10], Yanying Zheng[3,10], Wenli Fan[5], Chen Wu[1], Weiheng Zheng[1], Ke Fang[3], Shuhan Si[3], Shiqi Zhu[3], Yi Yang[3], Tao P. Zhong[6], Zhongzhou Yang[5], Ke Wei[7], Wei Xie[2,3], Naihe Jing[4,8,10,*], Zhuojuan Luo[2,3,*], Chengqi Lin[2,3,*]

[1]Basic Medicine Research and Innovation Center of Ministry of Education, Zhongda Hospital, School of Biological Science and Medical Engineering, Southeast University, Nanjing 210096, China.

[2]Co-innovation Center of Neuroregeneration, Nantong University, Nantong 226001, China.

[3]Basic Medicine Research and Innovation Center of Ministry of Education, Zhongda Hospital, Key Laboratory of Developmental Genes and Human Disease, School of Life Science and Technology, Southeast University, Nanjing 210096, China.

[4]Guangzhou Laboratory, Guangzhou 510005, China.

[5]State Key Laboratory of Pharmaceutical Biotechnology, Department of Cardiology, Nanjing Drum Tower Hospital, The Affiliated Hospital of Nanjing University Medical School and MOE Key Laboratory of Model Animal for Disease Study, Model Animal Research Center, Nanjing University, Nanjing 210061, China.

[6]Shanghai Key Laboratory of Regulatory Biology, Institute of Molecular Medicine, School of Life Sciences, East China Normal University, Shanghai 200241, China.

[7]Institute for Regenerative Medicine, Shanghai East Hospital, Shanghai Institute of Stem Cell Research and Clinical Translation, Shanghai Key Laboratory of Signaling and Disease Research, Frontier Science Center for Stem Cell Research, School of Life Sciences and Technology, Department of Molecular and Cellular Biology, Tongji University, Shanghai 200092, China.

[8]CAS Key Laboratory of Regenerative Biology, Guangdong Provincial Key Laboratory of Stem Cell and Regenerative Medicine, Guangzhou Institutes of Biomedicine and Health, Chinese Academy of Sciences, Guangzhou 510530, China.

[9]Institute for Stem Cell and Regeneration, Chinese Academy of Sciences, Beijing 100101, China.

[10]These authors contributed equally: Peng Xie, Xu Jiang, Jingjing He, Qingyun Pan, Xianfa Yang, Yanying Zheng

*To whom correspondence should be addressed at:

Chengqi Lin, Email: cqlin@seu.edu.cn

Zhuojuan Luo, Email: zjluo@seu.edu.cn

Naihe Jing, Email: njing@sibcb.ac.cn.

Abstract

The mammalian heart is formed from multiple mesoderm-derived cell lineages. However, it remains largely unknown when and how the specification of mesoderm towards cardiac lineages is determined. Here, we systematically depict the transcriptional trajectories toward cardiomyocyte in early mouse embryo, and characterize the epigenetic landscapes underlying the early mesodermal lineage specification by single-cell multi-omics analyses. The analyses also reveal distinct core regulatory networks (CRN) in controlling specification of mesodermal lineages. We further demonstrate the essential role HAND1 and FOXF1 in driving the earliest cardiac progenitors specification. These key transcription factors occupy at distinct enhancers, but function synergistically and hierarchically to regulate the expression of cardiac-specific genes. In addition, HAND1 is required for exiting from the nascent mesoderm program, while FOXF1 is essential for driving cardiac differentiation during MJH specification. Our findings establish transcriptional and epigenetic determinants specifying the early cardiac lineage, providing insights for the investigation of congenital heart defects.

Key words: Cardiogenesis; Single cell analysis; Epigenetics; Enhancer; HAND1.

Introduction

Heart development requires coordinated specification of multiple lineages, each characterized by serial cell fate determination events. Identifying the developmental trajectories is the key to understanding heart formation (Buckingham et al. 2005; Kelly 2023). In past decades, a stepwise determination of early cardiac lineage hierarchy has been primarily established (Parameswaran and Tam 1995; Abu-Issa and Kirby 2007). The current model designates cardiac progenitor cells into discrete pools, including the first and second heart field (FHF and SHF) (Buckingham et al. 2005), and a newly classified juxta-cardiac field (JCF) (Tyser et al. 2021). FHF mainly contributes to the left ventricle (LV) and the atria. SHF, located in a dorsal-medial region to FHF, progressively develops into cells in the right ventricle (RV), the outflow tract (OFT) and the atria (Cai et al. 2003). Interestingly, JCF contributes to not only epicardium and pericardium, but also cardiomyocytes (CMs) of LV and the atria (Tyser et al. 2021; Zhang et al. 2021).

Cardiac progenitors are mostly generated from the *Mesp1*-expressing (*Mesp1*$^+$) nascent mesoderm (NM) cells during gastrulation (Saga et al. 1999; Devine et al. 2014; Lescroart et al. 2014). Pioneering work has revealed that the developmental capacities of each cardiac progenitor pool are highly related to the spatial-temporal constriction during the specification of NM cells (Lescroart et al. 2018; Ivanovitch et al. 2021; Zhang et al. 2021). Temporally inducible lineage tracing indicates that E6.5 *Mesp1*$^+$ cells mostly contribute to LV, whereas E7.25 *Mesp1*$^+$ cells give rise to RV, atria, OFT, and inflow tracts (IFT) (Lescroart et al. 2018). It seems that early-streak stage NM cells differentiate into FHF pools, while late-streak stage NM cells relate to SHF progenitors. Interestingly, JCF population is also derived from the *Mesp1*$^+$ NM cells in the gastrula (Zhang et al. 2021). Recent studies on single-cell transcriptomic data of the late headfold stage embryos have revealed that JCF shares a number of molecular markers with FHF, but lacks *Nkx2.5* expression and exhibits specific *Mab21l2* expression (Tyser et al. 2021). However, unlike FHF cells, JCF cells are largely located at the embryonic-extraembryonic mesodermal interface, as revealed by the *Mab21l2* expression, rostrally to the *Nkx2-5* positive cardiac crescent region (Tyser et al. 2021). It remains unclear the molecular signaling underlying the early specification of NM cells into JCF and FHF population.

In this study, by bridging the transcriptional landscapes between the gastrula and the headfold stage in early mouse embryos, we systematically depict the transcriptional trajectories leading to CMs during early mouse development, and characterize the epigenetic landscapes that underlie early mesodermal lineage specification. The analyses reveal two dinstinct developmental trajectories towards CMs, namely the MJH trajectory (the *Hand1*-expressing early extraembryonic mesoderm – JCF and FHF – CM) and the PSH trajectory (the pharyngeal mesoderm cells – SHF – CM). Through single-cell multi-omics analysis, the core regulatory network (CRN) in MJH is identified, consisting of transcription factors (TFs) GATA4, TEAD4, HAND1 and FOXF1. Further functional analysis indicates that HAND1 and FOXF1 are activated sequentially, and both required for mesodermal specification and the expression of the MJH specific genes. Taken together, our study unveils the transcriptional and epigenetic dynamics during early cardiac specification, demonstrates the crucial roles of HAND1 and FOXF1 in driving early cardiac specification, and provides insights for the investigation of congenital heart defects.

Results

Transcriptional dynamics during the specification of early cardiac progenitors

To delineate the origin of cardiac progenitors, we constructed the E6.5-8.5 developmental trajectories using the published mouse gastrulation cell atlas by performing the Waddington-Optimal-Transport (WOT) analysis to infer ancestor-descendant fates of cells (Schiebinger et al. 2019), (Pijuan-Sala et al. 2019). CMs were used as trajectory endpoints and traced back to the E6.5 epiblast. Clear trajectory separation was observed within E7.5-7.75 (Figure 1A). Besides the pharyngeal mesoderm (PM) cell cluster at E7.75, a subset of E7.5 early extraembryonic mesoderm (EEM) cells (Zhang et al. 2021) was specifically identified in a distinct developmental trajectory. PM population was marked by the expression of *Isl1*, *Sfrp1*, *Tcf21*, *Tbx1* and *Irx3*, suggesting its relationship with the SHF progenitors; the EEM cells exhibited highly expressing *Hand1*, *Pmp22*, *Foxf1* and *Spin2c* (Figure S1A). In addition, cells along the EEM trajectory also expressed higher levels of the FHF signature genes, including *Tbx5* and *Hcn4*, suggesting their contribution to the FHF (Zhang et al. 2021). Compared with the PM trajectory, the EEM trajectory was mainly composed of cells in the later stages of cardiac development (Figure 1B and S1B). By the heart looping stage (E8.5), the two trajectories indeed exhibited distinct contributions to cardiac structures LV and OFT, respectively (Figure 1C).

Thus, we here refer to these two transcriptional trajectories as EEM-JCF/FHF (MJH) and PM-SHF (PSH) (Figure 1A). The spatial correlation of these two trajectories with heart fields was confirmed using the dataset from manually micro-dissected mesodermal cells in cardiac regions of E7.75-8.25 mouse embryos (Figure S1C) (Tyser et al. 2021). The MJH and PSH trajectories contained overlapping but temporally distinct cell types (Figure 1B). The separation of the two trajectories can be observed as early as E7.0 (Figure 1B). NM cells, marked by *Mesp1* and *Lefty2*, at E7.0 were more likely to be the multipotent progenitors of the PSH trajectory; whereas mixed mesoderm (MM) cells, marked by *Hand1* and *Msx2*, in later developmental stage and EEM cells tended to contribute to the MJH trajectory (Figures 1D and 1E).

We then systematically characterized the stage specific marker genes in the MJH and PSH trajectories. These two trajectories exhibited discrete and dynamic gene expression profiles during development (Figure 1F). We also observed relatively similar inhibitory Wnt and Nodal, as well

as active Fgf and Notch, signaling activities along the two trajectories (Figures 1G and S2A). Interestingly, the early stage of the MJH trajectory seems show higher Bmp and Yap signaling activities (Figure 1G). Temporal expression profiles of the *Bmp* genes indicated that *Bmp4*/*5*/*7* were dynamically expressed during cardiac specification, with *Bmp4* demonstrating higher MJH specificity and at least 0.5 days earlier activation (Figure S2B). Geo-seq data analysis indicated that *Bmp4* was highly specific to mesoderm, and enriched at the proximal mesodermal ends (layer 11 at E7.0, layer 9-10 at E7.5) with distinct anterior-posterior preference at E7.5 (Figure S2C). For the target genes of Bmp signaling, several genes (*Hand1*, *Car4*, *Arl4c* and *Pmp22*) showed MJH specific activation-to-repression dynamics, similar to *Bmp4* (Figures 1F and S2D).

Epigenetic signatures of the early MJH and PSH progenitors

To investigate the epigenetic regulation during cardiac cell fate decisions, we performed multi-omic analysis by combining single-nucleus RNA-sequencing (snRNA-seq) and scATAC-seq to generate paired, cell type specific transcriptome and chromatin accessibility profiles of 13,226 cells in E7.0 mouse embryos. The single-cell transcriptomic data were integrated with the published E7.0 mouse embryo cell atlas data, followed by label transfer and gene expression-based cell type identification (Figures S3A and S3B). For the scATAC-seq data, we scored the genome-wide ATAC activities with bin sizes of 10 kb prior to UMAP analysis, which yielded cell clusters similar to transcriptome-based analysis (Figure S3A).

9 clusters of cells were identified through clustering analysis at both transcriptional and epigenetic levels, which are NM cells (Clusters 0, 1 and 2), primordia germ cells (PGC, Cluster 4), hematoendothelial progenitors (Haem, Clusters 5 and 6), and EEM cells (Clusters 3, 7 and 8) (Figures 2A, 2B and S3C). RNA velocity also supported the four possible trajectories mentioned above for the earliest mesodermal cell specification (Figure 2C). WOT analysis revealed that Clusters 3, 7, and 8 showed intermediate to high probabilities of belonging to the MJH trajectory; pseudotime analysis indicated that Cluster 8 represented the late differentiated EEM populations (Figure S4A). Although Cluster 2 represented the relatively late stage of NM cell population by pseudotime analysis, Cluster 1, 0 and 2 demonstrated similar probabilities of belonging to the PSH trajectory (Figure S4A). Thus, the analyses further indicated that EEM cells and hematoendothelial

progenitors were clearly separated from the mesoderm, while the PSH trajectory related cells still remained at the early NM stage at E7.0.

We further analyzed the chromatin accessibilities of these cell clusters. Total 90,661 chromatin accessible elements (CAEs) were detected, 7,206 of which were differentially accessible elements (DAEs) across the 9 clusters (Figure 2d). The DAEs were annotated to their target genes by enhancer-promoter (EP) pairing analysis. Consistent with the clustering analysis based on gene expression (Figure S3C), DAVID functional term analysis revealed that the DAE target genes in Clusters 3, 7 and 8 , such as *Hand1*, *Foxf1*, *Bmp4* and *Msx1*, were mainly associated with heart morphogenesis, that those in Clusters 5 and 6, like *Tal1*, *Lmo2* and *Fli1*, were related to angiogenesis and vasculature development, and that those in Clusters 0, 1, 2, for examples, *T*, *Zic2*, *Lhx1* and *Gata6*, were enriched in gastrulation and mesoderm development (Figures 2D and 2E).

To characterize the spatiotemporal chromatin dynamics of the DAEs in MJH and PSH, we quantified the occupancies of the enhancer marks H3K4me1 and H3K27ac, as well as the promoter mark H3K4me3 at these DAEs across the E6.5-7.5 developmental stages(Yang et al. 2019). MJH/Cluster 8 and PSH/Cluster 2 specific DAEs could potentially function as enhancers and become activated at anterior regions of E7.5 embryos, as the DAEs were generally marked by H3K27ac and H3K4me1, but not H3K4me3 (Figure 2F). The enrichment of H3K4me1 at E7.0 and even earlier at E6.5 stage, along with the higher levels of H3K27ac at these DAEs at E7.5 stage, suggested that many of these DAEs could be dormant or inactive enhancers during earlier stages like E6.5, but primed for later activation during lineage specification (Figure 2F). Indeed, the integrated analysis on chromantin accessibility of the DAEs, shown by ATAC-seq, and their target gene expression levels supported that a large portion of the MJH/Cluster 8 DAEs were primed before the full activation of their target genes, like *Bmp4*, *Hand1* and *Foxf1* (Figure 2G). For example, seven DAEs associated with the *Bmp4* gene were identifited, three of which were primed at E7.0 as marked by low levels of H3K27ac but high levels of H3K4me1 (Figure 2H). Taken together, the combined transcriptome and chromatin accessability analysis further supported the early lineage segregation of MJH and the epigenetic priming at gastrulation stage for early cardiac genes.

Identification of lineage specific key TFs

An integrated analysis of motif enrichment at the DAEs and TF expression data allowed us to identify potential lineage specific key TFs. The PSH/Cluster 2 specific DAEs showed motif enrichment similar to the recognition sequences of known NM specific TFs, including GATA4, ZIC3, EOMES, OTX2, and LHX1 (Figure S4B). Binding sites for hematoendothelium-related TFs, such as GATA2, FLI1, JUNB, and SOX7, were enriched in the hematoendothelial progenitors/Cluster 6 DAEs. In contrast, the binding motifs of GATA4, HAND1, FOXF1 and TEAD4 were highly over-represented in the MJH/Cluster 8 specific DAEs (Figure 3A). Among those MJH-related TFs, GATA4 and TEAD4 showed similar expression and motif activities at Clusters 2, 7, 8 of both MJH and PSH lineages. HAND1 and FOXF1 demonstrated both strong motif activities and specific expression at Cluster 7 and Cluster 8. Interestingly, the expression of HAND1 and FOXF1 seemed relatively transient at NM and EEM cells, and then became downregulated at CM of E7.75 (Figure S4C).

Based on E7.0 single-cell multi-omics data analysis, we predicted a core regulatory network (CRN) centering on the four TFs (Figure 3b). Functional enrichment analyses indicated that this CRN could control key aspects of MJH specification, including Wnt signaling, epithelium cell migration, cell number maintenance, mesenchyme development, and cardiac development. In the CRN, GATA4 and TEAD4 controlled larger gene sets related to the transition from epiblast to mesodermal status, necessary for both MJH and PSH. HAND1 and FOXF1 co-regulated functionally more specific gene sets critical for differentiation to EEM status (Figure 3b). Consistently, most HAND1 and FOXF1 target genes were specifically expressed in EEM, in contrast to GATA4 and TEAD4 target genes (Figure 3b).

We also performed Chromatin immunoprecipitation sequencing (ChIP-Seq) analysis to profile the chromatin occupancies of HAND1 and FOXF1 in mesoderm (MES) and cardiac progenitor (CP) cells derived from the step-wise directed cardiomyocyte differentiation of mouse embryonic stem cells(Wamstad et al. 2012). We also collected published GATA4 ChIP-seq data(He et al. 2014) of E12.5 mouse embryonic heart, FLI1, ZIC2, ZIC3 and MESP1 ChIP-seq data(Lin et al. 2022) of 2.5 days EB differentiation. Direct comparison of ChIP-seq occupancy profiles with DAEs confirmed the specific enrichment of GATA4, HAND1, and FOXF1 at clusters 7 and 8 of MJH

lineages, Fli1 at Clusters 5 and 6, while MESP1 is specifically enrichment at mesoderm cell clusters (Figure 3C). We also noticed the enrichment of HAND1 at early Cluster 3-specific DAEs, while FOXF1 tends to show more speicifc enrichment at cardiac specific enhancers at later CP cells.

HAND1 and FOXF1 regulate the MJH specific genes

In order to further investigate the molecular roles of HAND1 and FOXF1 in MJH specification, we generated *Hand1* and *Foxf1* KO mouse embryonic stem cell (mESC) lines (Figures S5A-D), followed by *in vitro* mesoderm differentiation and RNA-seq analyses. 2,331 down-regulated and 1,714 up-regulated genes in *Hand1* KO mesoderm (MES) cells, and 870 down-regulated and 970 up-regulated genes in *Foxf1* KO MES cells with fold-change (FC) > 1.5 and *P*-value < 1e-5 were identified (Supplementary Table 2). To explore whether HAND1 and FOXF1 are required for the proper expression of the MJH related genes, we examined the expression of the signature genes of the 9 cell clusters in control , *Hand1* KO and *Foxf1* KO MES cells. First of all, over 90% of the cluster specific genes were detected in the control MES transcriptome, indicating that the *in vitro* differentiation model could be a reliable tool to study the regulation of these cluster specific signature genes (Figure 4A). Indeed, whole transcriptome cosine similarity analysis revealed that the *in vitro* differentiated MES cells were more close to MM and EEM cell state transcriptome-wide (Figure 4B). *Hand1* KO and *Foxf1* KO led to down-regulated expression of a large portion of the Clusters 3, 7 and 8 MJH marker genes, but up-regulated expression of many of the Clusters 0 and 1 PSH marker genes in MES cells (Figure 4A). Consistently, the cosine similarity suggested that *Hand1* and *Foxf1* depletion could lead to EEM differentiation defects (Figure 4B). In addition, many of the down-regulated MJH specific genes and up-regulated PSH specific genes were directly bound by HAND1 and FOXF1 (Figures 4A and S5E). The analysis indicated that HAND1 and FOXF1 could dually regulate MJH specification through directly activating the MJH specific genes and inhibiting the PSH specific genes.

Mutual regulation between HAND1 and FOXF1 in driving cardiac specific gene expression

We found that around 50% of the dysregulated genes in *Foxf1* KO MES cells were also dysregulated in *Hand1* KO MES cells, suggesting their synergistic function in transcriptional regulation (Figure 4C). For example, the key MJH specific genes, including *Hand1*, *Foxf1*, *Bmp4*,

Tbx20 and *Pmp22* were significantly down-regulated, while the epiblast genes *Dnmt3b*, *Sema6a* and *Fst*, and the NM specific genes *Otx2* and *Zic2* were substantially up-regulated in both KO cells (Figures 4C and S5E). Depletion of *Hand1* blocked the activation of *Foxf1* during cardic progenitor differentiation, and vice versa, while *Hand1* overexpression was able to activate *Foxf1* and the other MJH specific genes, and vice verse (Figures S6A-D).

The functional relevance between HAND1 and FOXF1 in target gene regulation could be attribuited to the enrichment of HAND1 at the *Foxf1* enhancers, and vice versa (Figure 4D). We then used CRISPR-Cas9 technology to delete the putative enhancers of *Hand1* and *Foxf1* (Figures S6E-F). Indeed, deletion of the HAND1-bound *Foxf1* enhancer (*Foxf1*-eH) abolished the activation of *Foxf1*; deletion of the FOXF1-bound *Hand1* enhancer (*Hand1*-eF) also significantly reduced the expression of *Hand1* during cardiac differentiation (Figures 4E and 4F). Importantly, the induction of the MJH specific genes *Bmp4*, *Pmp22* and *Spin2c* was severely impaired after deletion of either *Foxf1*-eH or *Hand1*-eF. Overexpression of HAND1 in the *Hand1*-eF KO cells and FOXF1 in the *Foxf1*-eH KO cells were able to rescue the levels of these MJH specific genes during cardiac differentiation. To further investigate the role of *Foxf1*-eH in *Foxf1* expression, we performed CRISPR activation (CRISPRa) assay to activate *Foxf1*-eH (Figures 4G). CRISPRa of *Foxf1*-eH led to a specific increase the expression of *Foxf1* and its downstream target genes, but not its neighboring genes (Figure 4H). Together, our data indicated that mutual regulation between HAND1 and FOXF1 could play a key role in MJH cardiac progenitor specification.

Hand1 KO leads to MES overproliferation but cell death after exiting from the MES status

Meta analysis demonstrated that HAND1 occupied the early Cluster 3 specific DAEs, while FOXF1 tended to show more specific enrichment at the late cardiac specific Clusters 7 and 8 enhancers (Figures 3C and 5A). We also noticed that the *Hand1* KO MES colonies were evidently much larger than those of WT control and *Foxf1* KO, though the same number of EB cells were seeded at equal density for MES differentiation (Figure 5B). While *Foxf1* KO barely affected cell proliferation rate, the count of the *Hand1* KO cells was substantially increased when the cells were differentiated from EB towards MES state (Figure 5C). The *Hand1* KO cells gradually lost viability upon *in vitro* cardiac lineage induction. Consistent with the increased proliferation rate observed, gene ontology (GO) analysis revealed that the genes involved in negative regulation of

proliferation and positive regulation of cell migration were specifically down-regulated in *Hand1* KO, but not *Foxf1* KO, MES cells (Figures 5D and S6G).

The *Foxf1* KO MES colonies derived from MES differentiation appeared phenotypically normal, but were not able to further differentiate into beating CMs (Figure 5B and Supplementary Video 1). The expression of the mature CM markers *Tnnt2*, *Myh6* and *Myh7* were also substantially lower after *Foxf1* KO (Figure S6H). To further examine the function of FOXF1 in cardiac progenitor specification, we performed RNA-seq analysis in control and the CP cells derived *Foxf1* KO mESCs. Gene Set Enrichment Analysis (GSEA) revealed the expression levels of the NM specific genes (like *Zic3*, *Pou5f1* and *Cited1*) and the PSH specific genes (like *Isl1*, *Ifitm1* and *Foxc2*) were remarkably up-regulated, while the expression levels of the MJH specific genes (like *Hand1*, *Spin2c* and *Tdo2*) and the early CM specific genes (like *Acta2*, *Tnnc1* and *Tnnt2*) were significantly reduced (Figure 5E). Thus, our data further supported the specific and synergistic roles of HAND1 and FOXF1 in MJH cardiac progenitor specification.

Genetic loss of *Hand1* blocks the specification of mesoderm along MJH

To further invesigate the roles of HAND1 in MJH specification *in vivo*, we generated floxed allele of *Hand1* by inserting loxP sites flanking the exon 1 of the *Hand1* gene. Genetic crosses of the *Hand1*$^{fl/fl}$ mice with *Mesp1-Cre* mice(Saga et al. 1999) allowed specific deletion of *Hand1* in mesodermal cells (Figure S7A). Consistently, *Foxf1* is also co-expressed in HAND1-positive EEM cells and its expression was also drastically down-regulated in MESP1-CRE driven *Hand1* conditional KO (*Hand1* CKO) embryos (Figure 6A). Mesodermal deletion of *Hand1* generally led to smaller embryos at E7.0 and also later stages (Figure S7B). The *Hand1* CKO embryos appeared to die by E9.5 due to embryonic turning failure and heart looping abnormality, mirroring the previously reported phenotype of *Hand1* KO mice (Firulli et al. 1998; Riley et al. 1998) (Figure 6B).

To assess how *Hand1* loss affects early mesoderm development *in vivo*, we analyzed the single-cell transcriptomics of control and *Hand1* CKO embryos at E7.0. Integrated analysis indicated the loss of EEM cells, but the abnormal accumulation of primitive streak (PS), NM and MM cells in *Hand1* CKO embryos (Figures 6C and 6D), which suggested that specific deletion of *Hand1* in

mesodermal cells strongly affected early mesoderm differentiation. Detailed analysis regarding the percentage of each cell type revealed the specific reduction of cell numbers from EEM, hematoendothelial progenitors, and ExE ectoderm cell clusters in *Hand1* CKO embryos (Figure 6D). We then compared the gene expression pattern for each cell cluster and calculated the significantly affected genes between Control and *Hand1* CKO embryos (Figure 6E). Consistently, EEM cell cluster was the most affected clusters upon *Hand1* loss (Figures 6E and S7C). Although the percentages of hematoendothelial progenitors and ExE ectoderm cells were reduced, the expression of both cell type specific marker genes did not seem affected drastically. To further illustrate the developmental progression of the mesodermal lineage, we performed paired URD lineage inference analysis(Farrell et al. 2018), further confirming the specific development block of NM specification towards EEM in MJH (Figure 6F). We also performed label transfer analysis to identify MJH and PSH cells from the E7.0 scRNA-seq data (Figure S7D). Our analysis showed that the fraction of MJH cells increased by over 2-fold, whereas the fraction of PSH cells remained unchanged (Figures S7E and S7F), supporting that *Hand1* deletion driven by MESP1-CRE blocked the MJH direction of mesoderm differentiation.

The abnormal accumulation of PS, NM and MM cells in *Hand1* CKO embryos appeared to be consistent with the phenotypes observed in *in vitro* mesoderm differentiation of *Hand1* KO mESCs (Figures 4B and 5B). Notably, the genes involved in negative regulation of proliferation and down-regulated in *Hand1* KO MESs were also reduced in the MJH, but not PSH, trjectory of E7.0 *Hand1* CKO embryos (Figure 7A). In addition, cell migration related genes were also affected in *Hand1*-depleted MES and embryos. To further validate this phenotype, we performed sequential DAPI staining on cryo-sectioned E7.0 control and *Hand1* CKO embryos, followed by cellular segmentation and cell density measurement (Figures 7B and 7C). The analysis revealed that the mesoderm cells near the extraembryonic region in *Hand1* CKO embryos were more compacted (Figures 7B’’, 7C’’, and 7D), while the distal region of the *Hand1* CKO embryos showed no obvious difference from the control embryos (Figures 7B’’’ and 7C’’’). In addition, reduced exocoelomic cavity (EC) size and increased number of mesodermal cells in extraembryonic region were also observed in *Hand1* CKO embryos (Figures 7B’ and 7C’). Hematoxylin and eosin (H&E) staining of E7.5 embryos also supported reduced embryo size and accumulated cells at

mesodermal regions upon loss of *Hand1* (Figure 7E). These data together establish HAND1 as a factor in promoting the specification of mesodermal cells toward MJH.

Discussion

In this study, we described the transcriptional trajectories and epigenetic landscapes of early cardiac specification event in mouse embryos, and identified the CRNs underlying the early mesodermal lineage specification. Mechanistically, we demonstrated that this earliest cardiac MJH specification event was tightly regulated by HAND1 and FOXF1. HAND1 and FOXF1 were mutually regulated, but also performed their respective functions in MJH cell fate determination. *In vitro* differentiation and *in vivo* mouse model analyses indicated that HAND1 was essential for exiting from NM program during cardiac specification. Depletion of FOXF1 impaired the capacity of mesodermal cells in cardiac specification (Figure 7F). In sum, our findings provided new insights into the transcriptional determinants that specify the early cardiac progenitors, paving the way for the identification of potential therapeutic targets for treating congenital heart defects.

Recent studies using scRNA-seq have reported the roadmaps of mammalian embryonic lineage development(Pijuan-Sala et al. 2019; Mittnenzweig et al. 2021; Qiu et al. 2022). Together with studies which focus on cardiac progenitors(de Soysa et al. 2019; Tyser et al. 2021; Zhang et al. 2021), several models have been proposed to explain the multi-lineage process of heart formation. In this study, we found significant distinction between the MJH and PSH trajectories at E7.5-7.75 and performed forward-backward tracing to achieve two non-overlapping trajectories. The two trajectories are consistent with the previous clonal analysis and also the HAND1+ cells lineage tracing by Zhang et al. (Meilhac et al. 2004). Importantly, we here identified specific trajectory-related gene cohorts throughout the whole process, shedding light on the molecular mechanisms by which HAND1 is crucial for promoting the exit of NM program during the early MJH specification process.

MESP1 serves as a master regulator in the establishment of the cardiac lineage. An analysis of previously published MESP1-regulated genes revealed that GATA4, HAND1 and FOXF1 were directly controlled by MESP1. GATA4 was rapidly induced by MESP1 within 12 hours, while HAND1 and FOXF1 were activated after 24 hours of MESP1 induction. On a pseudotime scale, we noticed a sequential-temporal expression pattern of GATA4, HAND1 and FOXF1 in MJH. Our transcriptional and epigenomic analyses suggested a sequential activation model of MESP1-GATA4-HAND1-FOXF1. However, it should be noted that MESP1 and GATA4 were activated

in both MJH and PSH. The process of cardiac lineage segregation is a complex one that may involve TF regulatory networks and signaling pathways. It has been reported that BMP signaling activated the expression of *Hand1* during heart formation (Zheng et al. 2021). Since Bmp4 displayed higher specificity for MJH, it might explain the activation of *Hand1*, and subsequent *Foxf1* activation in MJH, but not the PSH. Thus, HAND1 and FOXF1 might be subject to feed-forward activation by MESP1 and GATA4 in concert with BMP signalling, thereby promoting MJH cardiac specification. Future studies are worthwhile to further investigate how TFs work together with signaling pathways to promote cardiac lineage segregation.

We further demonstrated the synergistic roles of HAND1 and FOXF1 in early cardiac specification. *Foxf1*-/- mice were not able to survive beyond E10.0, with incomplete separation of splanchnic and somatic mesoderm, leading to abnormal coelom formation. Interestingly, FOXF1 marked the mesothelium lining (a monolayer epithelial lining of the exocoelomic cavity), the anterior distal part of which extends to the presumptive cardiac mesoderm(Fleury et al. 2015). Such an expression pattern is coincident with that of HAND1 in JCF(Tyser et al. 2021). Our studies showed that FOXF1 was indispensable for the specification of mesoderm toward early cardiac progenitors, through binding the MJH progenitor specific enhancers for their later activation. Together, the combined analyses on the developmental route of CMs and their transcriptional determinants will further enhance our understanding of the etiology behind congenital heart defects, ultimately providing insights into potential regenerative strategies for heart disease treatment.

Methods

Mice

All mouse experiments were approved by the Animal Care and Use Committee at Southeast University, and performed in accordance with institutional guidelines. Mice were housed in cages under SPF conditions and had free access to water and food. *Hand1*$^{fl/fl}$ mice were produced by Cyagen with loxP sites inserted into the regions surrounding exon 1 in the *Hand1* locus. *Hand1*$^{fl/+}$; *Mesp1-Cre* mice were generated by crossing *Hand1*$^{fl/fl}$ mice with *Mesp1-Cre* mice (Nie et al. 2015).

The *Hand1*$^{fl/fl}$ or *Hand1*$^{fl/+}$ female mice caged with male *Hand1*$^{fl/+}$; *Mesp1-Cre* mice. Females were screened for vaginal plugs following morning (E0.5). To obtain post-implantation embryos, female mice at 7.0 or 9.5 days post-coitum (d.p.c.) were executed and the uteri were dissected and transferred to a petri dish with PBS. For 7.0 d.p.c embryos, each decidua was carefully freed from the uterine muscle layers using properly sharpened forceps. Then the embryos were carefully separated from decidua. Reichart's membrane and the ectoplacental cone were also removed from the 7.0 d.p.c embryos. The uteri surrounding the 9.5 d.p.c embryos were cut open with a small incision, the embryos were genetly squeezed out, and then the amniotic membranes were removed. Images of the embryo were acquired on a stereo microscope (Mshot, MZ62; Olympus, SC180).

Genomic DNA for mouse genotyping was obtained from mouse tail biopsies. Genotyping of mouse embryos was performed with genomic DNA, which was obtained by collecting extra-embryonic regions subsequently digestion using Mouse Direct PCR Kit (Bimake, B40013). PCR reactions were used to detect the *Cre* transgene and the *Hand1* loxP site. Thermal cycle reactions were as follows: 3 min at 94 °C, 35 cycles of 30 s at 94 °C, 35 s at 60 °C, 45 s at 72 °C and a final 5 min extension at 72 °C. Primer sequences used in this study are listed in Supplementary Table 3.

Antibodies

Antibody against HAND1 (sc-390376) (WB: 1:1000, IF for embryos: 1:100, IF for cells: 1:200) was purchased from Santa Cruz. Antibody against FOXF1 (Abclonal, A13017) (WB: 1:2000, IF for embryos: 1:100, IF for cells: 1:500) was purchased from Abclonal. Antibody against HA (ChIP: 3 μg) was generated in house. Antibody against TUBULIN (66031-1-Ig) (WB: 1:50, 000) was

purchased from Proteintech. Goat anti-mouse IgG Alexa Fluor 488(A-11001) and goat anti-rabbit IgG Alexa Fluor 546 (A-11035) were purchased from Thermo Fisher Scientific.

Mouse ESC culture

Mouse E14 ESCs were maintained in DMEM (Hyclone, SH30243.01) supplemented with 15% FBS, 1 × nonessential amino acids (STEMCELL, 07600), 1 × GlutaMAX (Gibco, 35050-061), 1 × penicillin streptomycin solution (Sangon Biotech, E607011-0500), b-mercaptoethanol (ALDRICH), 0.1 μg/ml leukemia inhibitory factor (Novoprotein, C690), 3 μM CHIR99021 and 1 μM PD0325901 in gelatin-coated plates at 37 °C under 5% CO_2.

CRISPR-Cas9 guided KO

SgRNAs targeting *Hand1*, *Foxf1* and their enhancer sites were cloned into lentiCRISPR v2. These constructs were transfected into 70% confluent 293T cells together with 6 μg of psPAX2 packaging plasmids and 2 μg of pMD2.G envelope plasmids using Highgene (Abclonal, RM09014). The media was half-replaced with fresh DMEM supplemented with 10% FBS 6 h after transfection. The lentiviral supernatants were harvested at 24 h, 48 h, and 72 h post-transfection, filtered through 0.45 μm filters, and concentrated at 50,000 × g for 0.5 h. Mouse E14 ESCs were infected with concentrated lentiviral particles with polybrene (Sigma) at the concentration of 8 μg/ml. 2 μg/ml puromycin was used for selection for 48 h and individual colonies were picked and expanded in 48-well plates. The clones were screened with genomic PCR, and confirmed by TA cloning and Sanger sequencing. Oligo sequences used in this study are listed in Supplementary Table 3.

***In vitro* cardiac differentiation**

Mouse E14 ESCs were differentiated into embryoid bodies (EBs) at a density of 75,000 cells/ml in 6 cm dishes for 48 h in serum-free media (DMEM (Hyclone, SH30243.01), DMEM/F12 (1:1) (Gibco, 11320-033), 0.05% BSA (Sigma, A1933), 1 × GlutaMax (Gibco, 35050-061), B27 supplement (Gibco, 12587010), N2 supplement (Gibco, 17502048), supplemented with 50 mg/ml ascorbic acid (Alfa Aesar, 50-81-7) and 4.5×10^{-4} M monothioglycerol). EBs were dissociated into single cells and re-aggregated as MES cells for 40 h at 50,000 cells/ml in the presence of 5 ng/mL human VEGF (Novoprotein, C083) and 10 ng/ml human Activin A (Peprotech, 96-120-14-10) and 0.3 ng/ml human BMP4 (R&D, 5020-BP-010). MES cells were dissociated and plated as a

monolayer in gelatin-coated 12-well plate at 50,000 cells/ml in StemPro-34 (Gibco, 10639011) supplemented with 5 ng/mL VEGF (Novoprotein, C083), 10 ng/mL human basic FGF (Gibco, PMG0035) and 25 ng/mL FGF10 (R&D, 345-FG-250). CP cells were harvested after differentiation for 32 h. Contracting CMs can be observed after another 5 days. Differentiation stages were confirmed by the expression of marker genes.

Immunofluorescence

Mouse Embryos: Embryos were fixed in 4% PFA, then rinsed in PBS and incubated in 30% sucrose at 4 °C until sinking. Embryos were then embedded in OCT medium and snap-frozen in liquid nitrogen and stored at −80 °C. Sections were cut at a thickness of 10 μm. To perform IF, embryo sections were washed three times for 5 min each, then antigen repair was performed using citrate. The samples were permeated for 40 min with 0.3% TritonX-100 followed by washing three times with PBS for 5 min each. The samples were then blocked with ReadyProbes 2.5% Normal Goat Serum (Thermo) for 1 h at room temperature. The samples were incubated overnight at 4 °C with primary antibodies followed by washing three times with PBS for 10 min each. The samples were incubated with secondary antibodies for 1 h at room temperature, then washed three times with PBS for 10 min each. The samples were then incubated with DAPI at room temperature for 10 min followed by washing one time with PBS for 5 min. After the final wash, the samples were mounted with mounting buffer. Images were captured using a Zeiss 700 laser confocal microscope.

MES and CP cells were dissociated into single cells and fixed on 12-well plate cell slide with 4% PFA at room temperature for 15 min. The fixed cells were washed 3 times with PBS and permeabilized with 0.2% Triton X-100 for 5 min at room temperature. The cells were then blocked with PBS containing 2% BSA and 0.3% TritonX-100 for 1 h at room temperature. Appropriate dilution of primary antibody was added and cells were incubated overnight at 4 °C. After washing with PBS for 3 times, the cells were stained with secondary antibodies and DAPI for 1 h at room temperature followed by mounting on slides. Images were captured using a Zeiss 700 laser confocal microscope.

H&E staining

Whole E7.5 embryos were fixed overnight with 4% PFA, embedded vertically in clean paraffin, then sliced to obtain 7 μm paraffin sections. Standard hematoxylin and eosin (H&E) staining methods were used to stain the sections. The images of H&E staining were obtained on a microscope (Olympus, IX73).

Western blotting

Cells were washed twice in ice-cold PBS and incubated in 1 × SDS lysis buffer for 15 min at 95 °C. Lysates were pre-cleared by maximum speed centrifugation for 3 min, then separated by SDS-PAGE and transferred to polyvinylidene fluoride (PVDF) membrane. 5% non-fat dry milk was used for blocking and primary antibody was added. The membrane was incubated overnight at 4 °C, then washed, incubated with secondary antibody for 1 h at room temperature. ECL substrate was used for imaging by autoradiography.

Quantitative RT-PCR and bulk RNA-seq

Total RNA was extracted from cells using RNA isolater Total RNA Extraction Reagent (Vazyme). 500 ng of total RNA was used to synthesize cDNA using ABScript II RT Mix (Abclonal, RK20403). Resultant cDNA was diluted in water and 12.5 ng cDNA was used in each qRT-PCR reaction. Reactions were run on CFX96 (Bio-Rad) using 2 × Universal SYBR Green Fast qPCR Mix (Abclonal, RK21203). The relative expression levels of genes of interest were normalized to the housekeeping gene *Actin*. Each experiment contains at least three biological replicates. Primer sequences used in this study are listed in Supplementary Table 3. For RNA-seq, 1×10^6 MES or CP cells were harvested and RNA extraction was performed using Rneasy mini plus kit (Qiagen). 1 μg of total RNA was used for the construction of sequencing libraries and sequencing.

snRNA-seq

To prepare single cells for snRNA-seq, embryos at E7.0 were dissected in cold sterile 1 × PBS without Ca^{2+}, Mg^{2+} under a stereo microscope. Embryos were staged based on their morphology. The Reichert's membrane and ectoplacental cone were removed, and genotypic identification of embryos was carried out. Embryos were placed into a 1.5 ml microfuge tube and digested into

single cells using TrypLETM Express (Thermo) at 37 °C. Single-cell RNA sequencing was performed on single-cell suspensions using 10 × Genomics.

10 × Multiome library preparation and high throughput sequencing

Embryos staged at E7.0 were collected and washed with cooled 0.5% BSA/PBS for twice. Sufficient embryos were pooled and then subjected to 200 μL TrypLE for cell dissociation for 10 min at 37 °C with frequent gentle mixture. Single-cell suspension of embryos were then quenched and washed with 0.5% BSA/PBS, and finally filtered using 40 μm Flowmi cell strainer. The acquired single cell suspension were then subjected to nuclei isolation, library preparation by following the manufacturer's instruction. The library was sequenced on Novaseq 6000 platform with recommended sequencing depths and read lengths.

ChIP, ChIP-seq library preparation

$5 \times e^6$ cells were crosslinked with 1% formaldehyde for 10 min and quenched with 0.125 M glycine for 5 min at room temperature. Fixed cells were incubated in 0.5 ml lysis buffer (50 mM Tris-HCl [pH 8.0], 1 % SDS, 5 mM EDTA) for 10 mins on ice. After adding 1 ml dilution buffer (20 mM Tris-HCl [pH 8.0], 150 mM NaCl, 2 mM EDTA, 1% Triton X-100), chromatins were sonicated into 200-800 bp fragments using Bioruptor (Diagenode) and immunoprecipitated with protein A agarose beads and specific antibody at 4 ℃ for 12 h. Immunoprecipitates were washed with Wash Buffer I (20 mM Tris-HCl [pH 8.0], 150 mM NaCl, 2 mM EDTA, 1% Triton X-100, 0.1% SDS), Wash Buffer II (20 mM Tris-HCl [pH 8.0], 500 mM NaCl, 2 mM EDTA, 1% Triton X-100, 0.1% SDS), Wash Buffer III (10 mM Tris-HCl [pH 8.0], 0.25 M LiCl, 1 mM EDTA, 1% deoxycholate, 1% NP-40) and TE, respectively. After the final wash, DNA was eluted and reverse-crosslinked at 65 °C for at least 6 h. DNA was then purified and used for PCR amplification or ChIP-seq library preparation. ChIP-seq libraries were prepared with VAHTS Universal DNA Library Prep Kit for sequencing.

Data processing and quality control

Single cell multi-omics data: sequence alignment

We used Cell Ranger ARC software suite for the analysis of single cell multi-omics (ATAC & Gene Expression) data (https://support.10xgenomics.com/single-cell-multiome-atac-

gex/software/pipelines/latest/what-is-cell-ranger-arc). We applied the "cellranger-arc count" function for barcode counting, adapter/primer removal and sequence alignment. The processed reads were aligned to mm10 using the BWA-MEM algorithm. For ATAC sequencing data, BAM files were generated for downstream analysis. For Gene Expression (GEX) data, "cellranger-arc count" generated gene-barcode matrices were used for further analysis. Version of Cell Ranger ARC genomic sequence and gene annotation: refdata-cellranger-arc-mm10-2020-A-2.0.0.

snRNA-seq data

snRNA-seq datasets of the current study include: (1) E6.5-8.5 whole mouse embryos; (2) micro-dissected anterior cardiac regions of mouse embryos at early crescent to linear heart tube (~E7.75-8.25) stages. (3) GEX part of the single cell multi-omics data of E7.0 mouse embryos. (4) Control and *Hand1* CKO E7.0 mouse embryos.

We used R package 'Seurat' for QC and normalization purposes (Hao et al. 2021). Cells with abnormal sequencing depth (nFeature_RNA < 2000 or nCount_RNA > 1e5) or with high mitochondrial ratio (percent.mt > 5) were excluded. We used the 'SCTransform' to perform normalization, variance stabilization, and regression of cell cycle scores (using the 'CellCycleScoring' function). For dataset (1), we selected E7.0 samples, removed cells labelled as 'doublet' or 'stripped' and regressed out sequencing batches.

snATAC-seq data

Bam files of snATAC-seq from multiome data were processed using Snaptools (Fang et al. 2021) function 'snap- pre' to remove low-quality fragments (MAPQ < 30), over-sized fragments (length > 1,000 bp), secondary alignments and PCR duplicates. This function also generates cell-by-bin matrices of variable resolution (bin sizes: 1kb, 5kb, 10kb) for downstream analysis. The range of fragment coverage for bin selection was set between 500 and 20,000.

ChIP-seq data analysis

Adapter sequences were removed from Fastq files using trim_galore (v0.6.7) with default parameters. After trimming, ChIP-seq reads were aligned to the mm10 mouse genome using Bowtie2 (v2.3.5.1) (Langmead and Salzberg 2012) with '--no-mixed' and '--no-discordant'

parameters. The aligned files were sorted and converted to BAM format using SAMtools (v1.9). BigWig files were subsequently generated using deepTools bamCoverage (v3.5.0) (Ramirez et al. 2016), employing CPM normalization and ignoring duplicates. Peak calling was performed with MACS3 (3.0.0a6) (Zhang et al. 2008) for HAND1 (*Q*-value < 1e-5) and FOXF1 (*Q*-value < 1e-10) ChIP-seq data.

Tracing the CM, MJH and PSH trajectories

The trajectories of each in Figure 1 were inferred using the Waddington-OT Python package (v1.0.8) (Schiebinger et al. 2019) with a predefined starting cell set (E8.5 CM cells for tracing the CM trajectory, E7.5 EEM cells in the CM trajectory for tracing MJH trajectory, and E7.75 pharyngeal mesoderm cells in the CM trajectory for tracing the PSH trajectory), and cells of each trajectory are selected if WOT score > 0.0001. To specifically distinguish between MJH and PSH, the difference in the WOT score of the two trajectories was calculated, and if the difference is greater than 0, it belongs to the MJH trajectory and vice versa to the PSH trajectory. The WOT package was used with default parameters as in the Waddington-OT online tutorial (https://broadinstitute.github.io/wot/tutorial/).

Signaling pathway enrichment analysis

Potential signaling-activated/inhibited genes of Bmp, Yap, Wnt, Nodal, Notch and Fgf were collected from Peng et al. 2019 (Peng et al. 2019). Enrichment of signaling target gene sets was determined by the average expression levels of activated/inhibited genes.

Spatial mapping of single cells

Locations of mouse E7.0/7.5 mesodermal cells were inferred by comparison with the GEO-seq data, where each sample represents 5–40 cells with defined spatial locations. Transfer component analysis (TCA) (Pan et al. 2011) was performed to achieve shared representation of scRNA-seq and GEO-seq samples. Single cells were mapped to GEO-seq locations with the highest correlation coefficients.

Identification of pseudotime-dependent genes

Single-cell pseudotime trajectory analysis was performed using R package Monocle 2 (v2.22.0) (Trapnell et al. 2014) according to the online tutorials (http://cole-trapnell-lab.github.io/monocle-release/). Monocle object was directly constructed using Monocle implemented new Cell Data Set function from Seurat (v4.1.1) object, and Monocle implemented differentialGeneTest function was used to find highly variable genes for ordering. Based on these, we selected key and specific genes in MJH and PSH trajectory, respectively, and further visualized them in the heatmap using cell bin-by-gene matrix.

snRNA-seq data integration and label transfer

This research included data integration for the following datasets (dataset numbers in 'Data processing and quality control: snRNA-seq data'): (1) and (2) for comparison of the predicted trajectories and MJH cells; (1) and (3) for cell-type annotation of multiome single cells; (1) and (4) for cell-type annotation of Ctrl/*Hand1* CKO single cells. For multiome dataset, integration was performed by two steps: 1) whole embryo integration; 2) according to the predicted cell types of (1), mesoderm specific integration was done by selecting relevant cell types (NM, MM, EEM, Haem, PGC).

The integration and label transfer process follows the pipeline provided by Seurat (Hao et al. 2021): https://satijalab.org/seurat/articles/integration_introduction.html. 4,000 genes were selected for integration based on variable gene sets of individual datasets. We selected "SCT" as the normalization method for identification of integration or transfer anchors.

Clustering analysis of snRNA-seq data

We performed clustering analysis for cells of the integrated mesodermal lineage. Seurat (Hao et al. 2021) function "FindNeighbors" and "FindClusters" were applied to the Top 20 principle compoments with the following parameter setting: annoy.metric = "cosine", resolution = 0.95. This analysis resulted in nine clusters (C0-8), which is also used for snATAC-seq analysis.

FHF and SHF gene signature scores

For each gene set, we defined the average z-score normalized expression levels as the signature score per cell. The FHF and SHF gene sets were collected from Soysa et al. 2019 (de Soysa et al.

2019) Supplementary Table 1 (FHF: “FHF” genes of tab “Figure1de_n = 21,366 cells”; SHF: “MP” genes of tab “Fig 2ab_n = 2,103 cells”).

snATAC-seq data analysis

snATAC-seq bam files were combined for each cluster, C0-8, for identification of accessible elements (AE). AEs were then collected as a basic set of peak annotation. We used Snaptools (Fang et al. 2021) function ‘add_pmat’ to generate a cell-by-peak matrix (pmat), where the value of each element represent the accessibility per cell per peak. Diffusion map followed by UMAP analysis was performed to generate the snATAC-seq version of 2D data visualization.

Cluster specific AEs were identified using SnapATAC function ‘findDAR’. For analysis of C2-8 specific AEs, we used C1, which represents the least differentiated cell group, as the background cluster. For C0-1, we used cells from all other clusters as background. Cluster specific AEs were provided to HOMER (Heinz et al. 2010) function ‘findMotifsGenome.pl’ for motif analysis, and to deepTools (Ramirez et al. 2016) for plotting heatmaps of ChIP-seq data.

Definition of enhancer regulated target genes.

Enhancer-promoter (EP) pairs were predicted by SnapATAC function ‘predictGenePeakPair’ (Fang et al. 2021). This method performs logistic regression using peak accessibility (snATAC-seq) and expression (snRNA-seq) of neighboring genes to identify EP links. Candicate EP pairs need to be less than 50kb apart. Cluster specific target genes were defined as EP-associated genes of cluster specific AEs. Functional enrichment analysis was performed using R package clusterProfiler (Wu et al. 2021) (‘compareCluster’ function, ontology was selected as ‘BP’).

Analysis of TF activity

We analyzed TF activity, defined as the relative accessibility of AEs containing the motif sequence(Schep et al. 2017) of a TF, using R package chromVAR (https://greenleaflab.github.io/chromVAR/articles/Introduction.html). SnapATAC-generated cell-by-peak matrices were converted to ‘SummarizedExperiment’ format as the input of chromVAR. The TF activity is calculated by the ‘computeDeviations’ function by comparing the accessibility of motif-containing AEs with background peaks with similar GC content. Genomic coordinates of

motifs were acquired by the ‘getMatrixSet’ function and R package ‘JASPAR2020’. Synergy scores between TF pairs were computed by the ‘getAnnotationSynergy’ function.

Classification of activation modes of gene-enhancer pairs

We performed pseudotime trajectory analysis for E7.0 MJH trajectory (C0, C3, C7 and C8) in multiome using the abovementioned method. To further explore the underlying mesoderm developmental mechanism of enhancer clusters in regulating gene expression, we first built gene-enhancer pairs for preselected clusters based on snATAC-seq and snRNA-seq datasets. Secondly, we partitioned cells from E7.0 mesoderm lineage into pseudotime bins and calculated the cell bin-by- gene matrix of snRNA-seq and the cell bin-by-peak matrix of snATAC-seq, respectively. Finally, we divided activation modes of gene-enhancer pairs into three groups, fast, sync., and slow, according to the order of bins corresponding to their activation time.

Inference for URD lineage tree

To reconstruct branching developmental trajectory trees for E7.0 mesoendodermal cells (Ctrl and *Hand1* CKO), we used URD (v1.1.1) (Farrell et al. 2018). We used all cells assigned as epiblast as the root of the tree, and cells of clusters that contained the most differentiated cell-types at the latest pseudotime as the tips, where the CM branch was divided into MJH and PSH trajectories. By the movement of coordinates, the cells of Ctrl and *Hand1* KO are located on either side of the branch, respectively.

CRN construction and in silico KO

The CRNs based on multi-omics (scRNA + snATAC) data was constructed by SCENIC+ (v1.0.1) (ref) (details available via https://scenicplus.readthedocs.io/en/latest/pbmc_multiome_tutorial.html). CRN-based in-silico KO was conducted by SCENIC + module "scenicplus.simulation". In this step the expression level of a TF was set to zero and SCENIC + propagates the effect through CRN in an iterative manner to obtain the perturbed expression matrix. Cell-state transition vectors were generated and projected to the tSNE map using "plot_perturbation_effect_in_embedding" function.

Cell nucleus segmentation

We employed the cellpose (V2.1.1) (Stringer et al. 2021)algorithm for segmentation of DAPI staining for embyo transverse sections. The pre-trained CP model (--pretrained_model CP) was used to obtain the masks of images. We used option "--diameter 8" to resize the image to conform to the input parameters of the pre-trained model. We utilized the MorphoLibJ plugin of Fiji to obtain morphological metrics of the segmented nuclei. Finally, we utilized the VAA3D (2.938) (Peng et al. 2014) software to perform partitioning of the embryo, to identify cells belonging to the endoderm, mesoderm or epiblast.

Statistics and reproducibility

Numbers of biological replicates, statistical tests and *P*-values are reported in the figure legends. If not mentioned otherwise in the figure legend, statistical significance was determined using two-tailed Student's *t*-test, provided by GraphPad Prism9 statistical software.

Data availability

Sequencing (sc/snRNA-seq, snATAC-seq, ChIP-seq, and RNA-seq) data that support the findings of this study have been deposited in the Gene Expression Omnibus under accession numbers GSE245713. Previously published ChIP-seq data that were re-analyzed here are available under accession codes GSE165107 (MESP1, ZIC2 and ZIC3, 2.5-day EB), GSE47085 (HAND1, FLK+ MES cells), GSE52123 (GATA4, E12.5 mouse heart) and GSE69099 (FLI1, ES derived hemogenic endothelium). Previously published scRNA–seq data that were re-analyzed here are available under accession codes E-MTAB-6967 (ArrayExpress, E6.5-8.5 mouse embryos) and E-MTAB-7403 (ArrayExpress, micro-dissected heart-related samples of E7.75-8.5 mouse embryos). Previously published GEO-seq data that were re-analyzed here are available under accession codes GSE171588. All other data supporting the findings of this study are available from the corresponding author on reasonable request.

Acknowledgements

The authors are grateful to the Lin and Luo lab members for helpful discussion of this study. Studies in this manuscript were supported by funds provided by National Key R&D Program of China (2018YFA0800100 and 2018YFA0800101 to C.L.; 2018YFA0800103 to Z.L.), the National Natural Science Foundation of China (32030017 and 31970617 to C.L.; 31970626 to Z.L.; 32100529 to P.X.), Shenzhen Science and Technology Program (JCYJ20210324133602008 and JCYJ20220530160417038 to C.L.; JCYJ20210324133601005 and JCYJ20220530160416037 to Z.L.)

Declaration of interests

The authors declare that they have no conflicts of interest.

Figure legends

Figure 1: Inferred trajectories reflect two distinct development routes of CMs.

(A) Two distinct trajectories, the MJH trajectory and the PSH trajectory, were inferred during CM differentiation. UMAP layout from Pijuan-Sala et al. (Pijuan-Sala et al. 2019) is highlighted by cells belonging to the WOT predicted developmental trajectories for CM (left), EEM (upper middle) and PM (lower middle), respectively. UMAP layout for the CM trajectory with cells is colored by the difference between FHF- and SHF-gene signature scores. UMAP layout for the MJH or PSH trajectory is colored by cell types. Gene expression levels of *Hand1* (upper right) and *Isl1* (lower right) of cells along the CM trajectory is overlaid onto the above-mentioned UMAP layout. Epi, epiblast. PS, primitive streak. NM, nascent mesoderm. MM, mixed mesoderm. EEM, early extraembryonic mesoderm. PM, pharyngeal mesoderm. CM, cardiomyocyte.

(B) Independent component (IC) layout showing pseudotemporal trajectories for MJH trajectory (upper) and PSH trajectory (lower) cells, colored by cell type (left), pseudotime (middle) and developmental time (right).

(C) The MJH and PSH trajectories showing distinct contributions to cardiac structures. Spatial plot showing spots in cardiac subregions from E8.5 embryos (left) (Sampath Kumar et al. 2023). White lines denoting the region including outflow tract (OFT), ventricle (V) and Atria (A). 'Virtual' in situ hybridization (vISH) confirming spatial specificity of marker genes corresponding to cardiac subregions (middle). Dot plot showing expression difference in subregion specific genes in the MJH and PSH trajectories (right).

(D) Mesodermal lineage segregation at E7.0. UMAP layout for E7.0 CM trajectory cells is colored by cell type (left), trajectory (middle) and pseudotime (right).

(E) UMAP layout (same as d) showing the expression of the E7.0 marker genes of NM (*Mesp1*), MJH (*Hand1*) and PSH (*Lefty2*).

(F) Heatmap showing the expression of pseudotime-dependent genes for the MJH trajectory (right) and the PSH trajectory (left). Rows and columns represent genes and cell bins, respectively. Genes used for the heatmap are listed in Supplementary Table 1.

(G) Smoothened fitting curves showing expression levels of activated (solid line) and inhibited (dotted line) signaling markers in the MJH (red) and PSH (blue) trajectories.

Figure 2: Multi-omics analysis reveals epigenetic signatures of the early MJH and PSH progenitors.

(A-C) Clustering analysis of E7.0 single-cell multi-omics data and comparison between modalities of transcriptome (snRNA-seq) and chromatin accessibility (snATAC-seq). UMAP layout, using only snRNA-seq (A,C) or snATAC-seq (B) data, is colored by cluster identities (left) or cell types (right). For both (A) and (B), cluster identities are determined by snRNA-seq data. For (C), developmental directions, shown as arrows, are indicated by RNA-velocity analysis.

(D) Heatmap showing the activity of 7,206 differentially accessible elements (DAEs) between clusters. Rows and columns represent DAEs and clusters. Colors indicate levels of accessibility averaged among cells from each cluster. The length of the corresponding color bar on the left represents the number of DEAs. Representative DAE-associated genes are shown on the right side.

(E) Dot plot indicating functional enrichment of DAE-associated genes of each cluster.

(F) Epigenetic status of DAEs during mesodermal specification of E6.5-7.5 mice embryo. H3K4me1, H3K27ac and H3K4me3 profiles were averaged among DAEs of cluster C1 (NM), C2 (PSH-direction frontier) and C8 (MJH-direction frontier). Published H3K4me1, H3K27ac and H3K4me3 ChIP-seq data were collected from E6.5 epiblast, E7.0/7.5 posterior epiblast (P) and E7.5 anterior mesoderm (AM) (Yang et al. 2019).

(G) Smoothened heatmap showing dynamic gene expression (right) and enhancer accessibility (left) along E7.0 mesoderm pseudotime trajectories for gene-enhancer pairs. Dashed lines indicating the pseudo-temporal midpoint.

(H) Representative genome browser snapshots of ATAC/RNA-seq (aggregated gene expression and chromatin accessibility for each cluster), H3K4me1 and H3K27ac at the *Bmp4* locus. Putative enhancers status at E7.0 are highlighted by colors.

Figure 3: The CRN is identified centering on GATA4, HAND1, FOXF1 and TEAD4 in driving MJH specification.

(A) Identification of top MJH specific DNA-binding motifs and corresponding candidate TFs. The MJH specific DAEs were defined by comparing C8 with C1 snATAC-seq data using SnapATAC (Fang et al. 2021) 'findDAR' function. Motif calling was performed by the HOMER (Heinz et al. 2010) 'findMotifsGenome.pl' function. Motif activity (colored in red) and TF expression (colored in blue) levels of trajectory specific candidate TFs, are overlaid on the UMAP layout from Figure 2a.

(B) Core regulatory network (CRN) of E7.0 EEM cells. The network is composed of TFs (GATA4, HAND1, FOXF1 and TEAD4), TF binding regions (diamond shapes), target genes (dot shapes), colored lines (TFs to regions) and grey lines (regions to genes). Colors of genes and regions representing the log2 FCs of E7.0 EEM cells over other mesodermal cells, measured by scRNA-seq and snATAC-seq data, respectively. Functional enrichment terms of target genes are shown in boxes with subtitles indicating corresponding TFs. *Q*-values, using hyper-geometric tests, are shown in parenthesis.

(C) Heatmaps representing the enrichment of MESP1, ZIC2, ZIC3, FLI1, GATA4, HAND1 and FOXF1 across the DAEs of each cluster.

Figure 4: HAND1 and FOXF1 are mutually regulated and required for the expression of the MJH specific genes.

(A) Comparison of the genes affected by *Hand1* KO or *Foxf1* KO with cluster specific genes of E7.0 mesodermal cells. Dot plot showing that absolute (dot size) and relative (dot color) ratio of the cluster specific genes in WT, *Hand1* KO or *Foxf1* KO MES cells. >90% cluster specific genes were expressed in MES. Higher enrichment in C0-2 and lower enrichment in other clusters can be observed in *Hand1* KO or *Foxf1* KO MES cells. Bar plots showing the up- or down-regulated genes in *Hand1* KO or *Foxf1* KO MES cells. Lengths of bars representing the percentage of cluster specific genes which were up- or down-regulated. Dark colors indicating direct targets of *Hand1* (left) and *Foxf1* (right).

(B) Heatmap showing the transcriptomic similarity of MES cells and cell types of E7.0 mouse embryo. MES transcriptome data were generated using bulk RNA-seq. Cell-type specific transcriptomes of E7.0 mice were determined as the average of single-cell transcriptomes from each cell type. The gene set for comparison was defined as the collection of top 50 marker genes of each E7.0 cell type. Cosine similarity metric was used. Ant.PS, anterior primitive streak. Haem, haematoendothelial progenitors. Def.end, def.endoderm. Vis.end, visceral endoderm. Par.end, parietal endoderm. ExE.end, ExE endoderm. Surf.ect, surface ectoderm. ExE.ect, ExE ectoderm.

(C) Scatter plot showing gene expression FCs after *Hand1* KO or *Foxf1* KO. Dots representing genes with FC > 1.5 and adjusted P (P_{adj})-value < 1e-5 (Wald tests). Red and blue colors indicating genes co-activated/inhibited in *Hand1* KO and *Foxf1* KO cells. Correlation coefficient of FCs between *Hand1* KO and *Foxf1* KO is 0.74, P < 2.2e-16, *t*-test.

(D) Representative genome browser snapshots showing the localization of H3K27ac, H3K4me1, HAND1 and FOXF1 at the *Hand1* and *Foxf1* loci. The FOXF1-binding *Hand1* enhancer (*Hand1*-eF) and the HAND1-binding *Foxf1* enhancer (*Foxf1*-eH), for enhancer KO experiments, are highlighted.

(E-F) RT-qPCR showing that the reduction in RNA levels of the EEM marker genes after *Hand1*-eF KO can be rescued by HAND1 OE (e), and after *Foxf1*-eH KO can be rescued by FOXF1 OE.

(G) Cartoon illustrating target *Foxf1*-eH of by dCas9-VP64 and the genes in the vicinity of *Foxf1*-eH.

(H) RT-qPCR showing that the substantial increase in RNA levels of *Foxf1* and the FOXF1 target genes, but not the *Foxf1*-eH neighbouring genes in *Foxf1*-eH CRISPRa cells. Data are the

mean ± standard error of the mean from three independent experiments. Two-tailed unpaired Student's *t*-test was performed.

Figure 5: HAND1 and FOXF1 are required for the cardiac lineage specification.

(A) Meta plot analysis showing the occupancies of HAND1 (left) and FOXF1 (right) at the C3/7/8 MJH specific DAEs from Figure 2d.

(B) Bright field microscopic images of WT, *Hand1* KO and *Foxf1* KO cells at MES, early CP, late CP and CM stages. Scale bar: 100 μm.

(C) Growth curve showing numbers of WT, *Hand1* KO and *Foxf1* KO cells counted at different time intervals during EB to MES differentiation. Data are the mean ± standard error of the mean from three independent experiments. Two-tailed unpaired Student's *t*-test was performed.

(D) Enriched GO terms of the genes up- or down-regulated after *Hand1* KO. One-sided Fisher's Exact test with Benjamini-Hochberg multiple testing correction was performed.

(E) GSEA showing the distribution of the marker genes within the ranking of *Foxf1* KO affected genes of *in vitro* differentiated CP cells (FDR calculated by permutation tests). *Foxf1* KO affected genes were ranked from up- (red) to down-regulation (blue).

Figure 6: *Hand1* KO in mesodermal cells blocks MJH specification in mouse embryos.

(A) Immunofluorescence staining showing a substantial reduction in protein levels of HAND1 and FOXF1 at the embryonic-extraembryonic boundary transverse sections (indicated by dashed lines and arrows) of E7.0 *Hand1* CKO embryos. Bright filed images (lateral view) of corresponding embryos are shown on the left side. The distance for each section to the distal tip of the embryo is labelled at the upper right corner for each image. Scale bars: 100 μm (bright field images, left) and 20 μm (transverse sections, right).

(B) The bright field images of E9.5 Control (Ctrl) and *Hand1* CKO mouse embryos. The arrows indicating the embryonic heart (h) and head folds (hf). Scale bar: 500 μm.

(C) UMAP layout of integrated E7.0 mouse embryo scRNA-seq data. Integration was performed using the scRNA-seq data of Ctrl and *Hand1* CKO mice. Colors indicating cell types. Dashed lines emphasizing cells with increased (red) or decreased (yellow) numbers in *Hand1* CKO mice.

(D) Bar plot showing the percentage of each cell type of Ctrl and *Hand1* CKO mice.

(E) Dot plot showing marker gene expression in Ctrl and *Hand1* CKO mice. Red highlighting markers of MM and EEM cell type.

(F) URD inferred trajectory tree revealing the developmental hierarchy of E7.0 mesoderm cells (Ctrl and *Hand1* CKO snRNA-seq), colored by cell types. Ctrl and *Hand1* CKO cells are distributed on both sides of the URD tree trunk, with Ctrl cells on the left and *Hand1* CKO cells on the right.

Figure 7: HAND1 is required for exiting from the NM program.

(A) Co-regulated changes in the genes related to negative regulation of cell proliferation (left) and positive regulation of cell migration (right) *in vivo* and *in vitro*. Heatmap showing the fold changes (FC) of those co-regulated genes after *Hand1* KO and *Foxf1* KO in MES cells *in vitro* (top). Dot plot showing expression levels of those co-regulated genes after *Hand1* KO in the MJH and PSH trajectories *in vivo* (bottom).

(B-C) DAPI staining in the transverse sections of E7.0 Ctrl (b) and *Hand1* CKO (c) embryos. The distance for each section to the distal tip of the embryo was labelled at the upper right corner for each image. Dashed white lines denoting locations of the exocoelomic cavity (EC) and NM.

(D) Violin plot showing the distance between neighboring mesoderm cells in the transverse sections of E7.0 Ctrl and *Hand1* CKO embryos. *P*-value was calculated using one-sided Mann-Whitney U test.

(E) H&E staining showing reduced embryo size and accumulation of mesodermal cells of E7.5 *Hand1* CKO mouse embryos. Scale bars: 100 μm.

(F) Working model of early cardiac lineage differentiation. Cardiac fate specification initiates around E6.75-7.0 by segregation of the MJH and PSH trajectories. At E7.0, multipotent progenitor cells in MJH lineage present *Hand1*+ mixed mesodermal (MM) status, in contrast to PSH cells showing *Lefty2*+ nascent mesodermal (NM) status. MJH and PSH specifically contribute to JCF and SHF, respectively, while they both contribute to the formation of early heart tube (HT). HAND1 and FOXF1 bind to enhancers, regulate the MJH specific genes, and drive mesodermal differentiation toward MJH direction. *Hand1* deletion led to blocked MJH specification and accumulation of early mesodermal cells.

Figure S1: Data integration showing the developmental trajectories of cardiac progenitors

(A) Gene expression levels of the PSH (upper), MJH (middle) and FHF markers (lower) overlaid on the UMAP layout of the CM trajectory. Only cells belonging to the CM trajectory are shown.

(B) Violin plots showing the distribution of mature myocardium markers expression levels in E8.5 CM cells of the MJH and PSH trajectories.

(C) Fraction of labels transferred from Tyser et al. (Tyser et al. 2021) for E7.5 EEM cells and E7.75 PM cells.

Figure S2: Differential gene expression and signaling activaity in MJH and PSH

(A) Smoothened fitting curves showing expression levels of activated (solid line) and inhibited (dotted line) signaling target genes in MJH (red) and PSH (blue).

(B) Dynamic expression of *Bmp4*/*5*/*7* in MJH and PSH between E7.0-E8.5 stages.

(C) Corn plots showing spatial MJH (upper) and PSH single cell mapping at the E7.0 (left) and E7.5 (right) stages. Columns representing micro-dissected locations in germ layers and rows representing distal (slice 2) to proximal ends (slices 10/11) of the mouse embryos. Colors indicating the number of single cells mapped to each location, or the aggregated expression level of *Bmp4*. EA, anterior endoderm; EP, posterior endoderm; M, whole mesoderm; MA, anterior mesoderm; MP, posterior mesoderm; A, anterior ectoderm; P, posterior ectoderm; L, left lateral ectoderm; R, right lateral ectoderm.

(D) Dynamic expression of the Bmp signaling target genes *Car4* and *Arl4c* in MJH and PSH between E7.0-E8.5 stages.

Figure S3: Data integration of E7.0 multi-omics snRNA-seq with reference scRNA-seq

(A) UMAP layout of E7.0 snRNA-seq or snATAC-seq data. UMAPs of snRNA-seq was generated by integrating published (Pijuan-Sala et al. 2019) and multi-omics data of this study. Cells are colored by cell types.

(B) Dot plot showing marker gene expression in reference and multi-omics dataset.

(C) Heatmap showing expression levels of marker genes across mesodermal clusters of E7.0 mouse embryos.

Figure S4: Identification of the key lineage specific TFs

(A) UMAP layout of the MJH (C0/3/7/8) and PSH (C1/0/2) developmental trajectories. Color shades indicating pseudotime for developmental stages. Dot plots showing the marker gene expression for MJH specific clusters (C3/7/8) and PSH specific clusters (C1/0/2) in snRNA-seq.

(B) Identification of top PSH (upper)/Haem (lower) specific DNA-binding motifs and corresponding candidate TFs. The PSH/Haem specific DAEs were defined by comparing C2/C6 with C1 snATAC-seq data using SnapATAC (Fang et al. 2021) 'findDAR' function. Motif calling was performed by the HOMER (Heinz et al. 2010) 'findMotifsGenome.pl' function. Motif activity (colored in red) and TF expression (colored in blue) levels of trajectory specific candidate TFs, are overlaid on the UMAP layout from Figure 2a.

(C) Dynamic expression of *Gata4*, *Tead4*, *Hand1* and *Foxf1* in MJH and PSH between E7.0-E8.5 developmental stages.

Figure S5: Generation of the *Hand1* and *Foxf1* KO ESC lines

(A,C) Schematic diagram of the positions of sgRNAs targeting the CDS of *Hand1* (A) and *Foxf1* (C).

(B,D) Genomic PCR analyses using the primer sets flanking the cleavage sites verifying the genomic DNA deletion of *Hand1* (B) and *Foxf1* (D).

(E) Heatmap showing expression levels of the marker genes across mesodermal clusters of E7.0 mouse embryos (left). Bar plots showing expression FC upon *Hand1* and *Foxf1* KO (right). Asterisks indicating direct binding by the corresponding TFs.

Figure S6: Mutual regulation between HAND1 and FOXF1

(A-D) RT-qPCR showing the levels of HAND1 and FOXF1 in *Hand1* and *Foxf1* KO, the EEM marker genes (*Foxf1*, *Bmp4*, *Pmp22* and *Spin2c*) after HAND1 and FOXF1 OE.

(E-F) Genomic PCR analyses using the primer sets flanking the cleavage sites verifying the genomic DNA deletion of the *Hand1* enhancer (a) and the *Foxf1* enhancer (c).

(G) Enriched GO terms of the genes up- or down-regulated after *Foxf1* KO. One-sided Fisher's Exact test with Benjamini-Hochberg multiple testing correction was performed.

(H) RT-qPCR showing that the expression levels of *Myh6*, *Myh7* and *Tnnt2* at CM stage are impaired by *Foxf1* KO. Data are the mean ± standard error of the mean from three independent experiments. Two-tailed unpaired Student's *t*-test was performed.

Figure S7: HAND1 is required for the expression of the EEM specific genes *in vivo*

(A) Schematic diagram showing strategy for the mesodermal cell specific *Hand1* KO embryo generation.

(B) Bright field images of representative E7.0 Ctrl and *Hand1* CKO embryos. Scale bar: 0.1 mm.

(C) UMAP layout as in Figure 6C. Colors indicating expression levels of the marker genes of Epi, PS, NM and EEM.

(D-E) Projection of E7.0 scRNA-seq onto the reference UMAP structure from Figure 1d. Reference UMAP layout for E7.0 CM trajectory cells colored by cell type (b) and trajectory (c).

(F) Bar plot showing the percentage of the MJH and PSH trajectories in NM of Ctrl and *Hand1* CKO mice.

Supplemental Tables

Table S1.1: Pseudotime-dependent genes for MJH/PSH trajectoyies. Related to Figure 1F

Gene	Cluster
Mixl1	Common
Tdgf1	Common
T	Common
Eomes	Common
Mesp1	Common
Pou5f1	Common
Car2	Common
Ccnd1	Common
Fgf3	Common
Sgk3	Common
Tbx3	Common
Phlda2	Common
Dkk1	Common
Hoxb2	Common
Meg3	Common
Vim	Common
Nrp1	Common
H19	Common
Hand2	Common
Rem1	Common
Bmp5	Common
Hapln1	Common
Cd24a	Common
Ephb1	Common
Sfrp5	Common
Gata5	Common
Mef2c	Common
Sox4	Common
Nkx2-5	Common
Mesp2	PSH specific
Sp5	PSH specific
Frzb	PSH specific
Arl4d	PSH specific
Gsc	PSH specific

Cyp26a1	PSH specific
Lefty2	PSH specific
Lhx1	PSH specific
Dll3	PSH specific
Pmaip1	PSH specific
Fam212a	PSH specific
Fgf5	PSH specific
Lhfp	PSH specific
Zic3	PSH specific
Cpa2	PSH specific
Sfrp1	PSH specific
Crabp1	PSH specific
Tbx1	PSH specific
Tcf21	PSH specific
Apoe	PSH specific
Hoxb3os	PSH specific
Pard6g	PSH specific
Isl1	PSH specific
Meis1	PSH specific
Aldh1a2	PSH specific
Fam213a	PSH specific
Tspan7	PSH specific
Hoxb1	PSH specific
Hoxa1	PSH specific
Dbn1	PSH specific
Vstm2b	MJH specific
Msx2	MJH specific
Hand1	MJH specific
Ppic	MJH specific
Msx1	MJH specific
Foxf1	MJH specific
Spin2c	MJH specific
Pmp22	MJH specific
Bmp4	MJH specific
Arl4c	MJH specific
Hoxd1	MJH specific
Tdo2	MJH specific
Krt18	MJH specific
Krt8	MJH specific

Mest	MJH specific
Hsd11b2	MJH specific
Dlk1	MJH specific
Tmem108	MJH specific
Csrp1	MJH specific
Tbx5	MJH specific
Mab21l2	MJH specific
Crip2	MJH specific
Tgfb1i1	MJH specific
Rbm38	MJH specific
Myocd	MJH specific
Wnt2	MJH specific
Tnnc1	MJH specific
Tnnt2	MJH specific
Acta2	MJH specific
Actc1	MJH specific
Myl7	MJH specific
Ttn	MJH specific
Hcn4	MJH specific
Myl9	MJH specific
Alcam	MJH specific
Hspb1	MJH specific
Nppb	MJH specific
Tnni3	MJH specific
Nppa	MJH specific

Table S1.2: Gene-enhancer pairs in E7.0 mesoderm pseudotime trajectories. Related to Figure 2G

Gene	Peak
Bmper	chr9:23205101-23205836
Hs3st3b1	chr11:63793400-63793901
Daam1	chr12:71813806-71814148
Pik3ap1	chr19:41388870-41389628
Rbm24	chr13:46522878-46523765
Dnah2	chr11:69437127-69437715
Masp1	chr16:23308079-23308586
Nrp1	chr8:128362384-128363365
Gfpt2	chr11:49781554-49782328
Nfatc2	chr2:168553368-168553873
Nfatc2	chr2:168633039-168633743
Tbx3	chr5:119588186-119589099
Nectin2	chr7:19695082-19695480
Rbm20	chr19:53670532-53671133
P4ha2	chr11:54064566-54064817
Kdr	chr5:76008228-76008806
Foxf1	chr8:120859927-120860544
Runx1	chr16:92685575-92686199
Slc6a6	chr6:91546003-91546701
Itga9	chr9:118774313-118774658
Tmem88	chr11:69510823-69511366
Vldlr	chr19:27183395-27183815
Cxcr4	chr1:128551753-128552340
Frmd6	chr12:70766970-70767397
Uaca	chr9:60787496-60788106
Zfhx3	chr8:108606479-108607224
Cgnl1	chr9:71749980-71750457
Kdm6b	chr11:69474662-69475132
Krt18	chr15:102013681-102013965
Rbfox2	chr15:77313482-77314091
Cgnl1	chr9:71709031-71709501
Smad7	chr18:75295165-75296030
Gm15511	chr9:69234348-69234819
Bmp4	chr14:46582969-46583613
Tbx20	chr9:24848198-24848669

Bmp2	chr2:133429498-133430016
Ryr2	chr13:12030416-12030844
Frem1	chr4:83095438-83095824
Tbx2	chr11:85803990-85804510
Klf6	chr13:5824290-5824668
Fpgs	chr2:32655607-32656216
St8sia1	chr6:142831256-142831930
Smad6	chr9:63919240-63919570
Kcnma1	chr14:23902557-23903307
Ackr3	chr1:90240337-90240673
Gm15222	chr14:46582969-46583613
Nrp1	chr8:128251495-128252057
Arfgef1	chr1:10285267-10285743
Dok4	chr8:94900700-94901649
Kif26b	chr1:178645037-178645334
Alpk3	chr7:81057414-81058331
Tpm1	chr9:67163861-67164376
Tbx20	chr9:24888287-24888799
Capn5	chr7:98149520-98150564
Rubie	chr14:46578136-46578796
Hand1	chr11:57929446-57929965
Bmp5	chr9:76007435-76007997
Podxl	chr6:31587404-31587997
Ano1	chr7:144786403-144786986
Mest	chr6:30703300-30704166
Gli2	chr1:118904950-118905383
Afdn	chr17:13709118-13709846
Ksr1	chr11:79123505-79123959
Rubie	chr14:46573109-46573707
St3gal6	chr16:58538961-58539278
Gm15511	chr9:69270897-69271224
Map3k5	chr10:20001907-20002282
Dok4	chr8:94892725-94893264
1700017B05Rik	chr9:57354263-57355026
Peg10	chr6:4634494-4634975
Rubie	chr14:46612475-46612905
Lypd6	chr2:50175810-50176459
Nckap5	chr1:126719707-126720255
Kif26b	chr1:178661078-178661894

Ahnak	chr19:9050275-9050663
Frem1	chr4:82959967-82960424
Hapln1	chr13:89401161-89401629
Col1a1	chr11:95004154-95004501
Cmtm7	chr9:114541247-114541587
Notch2	chr3:97889960-97890632
Hspa12b	chr2:131140351-131140939
Morc4	chrX:139875251-139875622
Pdgfb	chr15:79950260-79951054
Pdgfb	chr15:80000585-80000947
Map1b	chr13:99679373-99679831
Mvb12b	chr2:33877943-33878692
Adgra2	chr8:26887106-26887393
Wt1	chr2:105153091-105153686
Nfatc2	chr2:168589929-168591368
Adgra2	chr8:27088697-27089310
Tmem108	chr9:103805424-103805892
Ppp1r13b	chr12:111896858-111897524

Table S2. *Hand1*- and *Foxf1*-KO affected genes in MES cells. Attached as an excel file.

Table S3: Primers/oligos used in the current study

	Gene	Forward	Reverse
RT-qPCR primer	*Actin*	CTGTCGAGTCGCGTCCACC	CGCAGCGATATCGTCATCCA
	Myh6	GCCCAGTACCTCCGAAAGTC	GCCTTAACATACTCCTCCTTGTC
	Myh7	ACTGTCAACACTAAGAGGGTCA	TTGGATGATTTGATCTTCCAGGG
	Tnnt2	CAGAGGAGGCCAACGTAGAAG	CTCCATCGGGGATCTTGGGT
	Hand1	ACGCACATCATCACCATCAT	CTACTGCGGTGGTAGGTGGT
	Foxf1	ACGCCGTTTACTCCAGCTC	CGTTGTGACTGTTTTGGTGAAG
	Bmp4	TTCCTGGTAACCGAATGCTGA	CCTGAATCTCGGCGACTTTTT
	Pmp22	CCGCAGCACAGCTGTCTTT	AGCAGATTAGCCTCAGGCACAA
	Spin2c	CACCACATTGGCTCTACAACC	CACGATGCTCCTACGGGAT
	Mthfsd	TGAGAAAGGCTGGCGAATTGG	GGGGATGTCTACGACCTGG
	Foxc2	AACCCAACAGCAAACTTTCCC	GCGTAGCTCGATAGGGCAG
	Foxl1	GAGCAGAGGGTCACACTGAAC	CTTCCTGCGCCGATAATTGC
	Fbxo31	CATGCGGTTCAAGCCACTG	GTCTGGTTACACTTGGTGGAG
sgRNA for genomic deletion	*Hand1* sgRNA1	TGCCGGCGGGCCACCACCTA	
	Hand1 sgRNA2	ACTTGATGGACGTGCTGGCC	
	Foxf1 sgRNA1	GATGTCCGCGCCCGACAAGC	
	Foxf1 sgRNA2	CCCCTAACGGATTATTTGTA	
	Hand1-eF sgRNA1	CGCGTCATAACCTATAGGGC	
	Hand1-eF sgRNA2	AAGTGTCGGCCGGTGGCGAT	
	Foxf1-eH sgRNA1	TACGTCCTGGACCTGCTAAC	
	Foxf1-eH sgRNA2	AGGCTGGCTGCGTGCACGTA	
sgRNA for CRISPRa	Ctrl sgRNA	ATGCGTCAGTCGACTGATGC	
	Foxf1-eH sgRNA1	TACGTCCTGGACCTGCTAAC	
	Foxf1-eH sgRNA2	AGTTAGCAGGTCCAGGACGT	
mice genotyping primer	*Hand1*-CKO-5'	GTTGCCTACAGAAACCTTCAAGAGG	ATGGTGATGATGTGCGTAGCTG
	Hand1-CKO-3'	TTTTGGGTCTTCTCCAGTTTGAGT	GACCCCGAGGGTCAGATAAAAG
	Mesp1-Cre	TTCTGGAAGGGGCCCGCTTCA	GCCTGTTTTGCACGTTCACCG

Reference

Abu-Issa R, Kirby ML. 2007. Heart field: from mesoderm to heart tube. *Annu Rev Cell Dev Biol* **23**: 45-68.

Buckingham M, Meilhac S, Zaffran S. 2005. Building the mammalian heart from two sources of myocardial cells. *Nat Rev Genet* **6**: 826-835.

Cai CL, Liang X, Shi Y, Chu PH, Pfaff SL, Chen J, Evans S. 2003. Isl1 identifies a cardiac progenitor population that proliferates prior to differentiation and contributes a majority of cells to the heart. *Dev Cell* **5**: 877-889.

de Soysa TY, Ranade SS, Okawa S, Ravichandran S, Huang Y, Salunga HT, Schricker A, Del Sol A, Gifford CA, Srivastava D. 2019. Single-cell analysis of cardiogenesis reveals basis for organ-level developmental defects. *Nature* **572**: 120-124.

Devine WP, Wythe JD, George M, Koshiba-Takeuchi K, Bruneau BG. 2014. Early patterning and specification of cardiac progenitors in gastrulating mesoderm. *Elife* **3**.

Fang R, Preissl S, Li Y, Hou X, Lucero J, Wang X, Motamedi A, Shiau AK, Zhou X, Xie F et al. 2021. Comprehensive analysis of single cell ATAC-seq data with SnapATAC. *Nat Commun* **12**: 1337.

Farrell JA, Wang Y, Riesenfeld SJ, Shekhar K, Regev A, Schier AF. 2018. Single-cell reconstruction of developmental trajectories during zebrafish embryogenesis. *Science* **360**.

Firulli AB, McFadden DG, Lin Q, Srivastava D, Olson EN. 1998. Heart and extra-embryonic mesodermal defects in mouse embryos lacking the bHLH transcription factor Hand1. *Nat Genet* **18**: 266-270.

Fleury M, Eliades A, Carlsson P, Lacaud G, Kouskoff V. 2015. FOXF1 inhibits hematopoietic lineage commitment during early mesoderm specification. *Development* **142**: 3307-3320.

Hao Y, Hao S, Andersen-Nissen E, Mauck WM, 3rd, Zheng S, Butler A, Lee MJ, Wilk AJ, Darby C, Zager M et al. 2021. Integrated analysis of multimodal single-cell data. *Cell* **184**: 3573-3587 e3529.

He A, Gu F, Hu Y, Ma Q, Ye LY, Akiyama JA, Visel A, Pennacchio LA, Pu WT. 2014. Dynamic GATA4 enhancers shape the chromatin landscape central to heart development and disease. *Nat Commun* **5**: 4907.

Heinz S, Benner C, Spann N, Bertolino E, Lin YC, Laslo P, Cheng JX, Murre C, Singh H, Glass CK. 2010. Simple combinations of lineage-determining transcription factors prime cis-regulatory elements required for macrophage and B cell identities. *Mol Cell* **38**: 576-589.

Ivanovitch K, Soro-Barrio P, Chakravarty P, Jones RA, Bell DM, Mousavy Gharavy SN, Stamataki D, Delile J, Smith JC, Briscoe J. 2021. Ventricular, atrial, and outflow tract heart progenitors arise from spatially and molecularly distinct regions of the primitive streak. *PLoS Biol* **19**: e3001200.

Kelly RG. 2023. The heart field transcriptional landscape at single-cell resolution. *Dev Cell* **58**: 257-266.

Langmead B, Salzberg SL. 2012. Fast gapped-read alignment with Bowtie 2. *Nat Methods* **9**: 357-359.

Lescroart F, Chabab S, Lin X, Rulands S, Paulissen C, Rodolosse A, Auer H, Achouri Y, Dubois C, Bondue A et al. 2014. Early lineage restriction in temporally distinct populations of Mesp1 progenitors during mammalian heart development. *Nat Cell Biol* **16**: 829-840.

Lescroart F, Wang X, Lin X, Swedlund B, Gargouri S, Sanchez-Danes A, Moignard V, Dubois C, Paulissen C, Kinston S et al. 2018. Defining the earliest step of cardiovascular lineage segregation by single-cell RNA-seq. *Science* **359**: 1177-1181.

Lin X, Swedlund B, Ton MN, Ghazanfar S, Guibentif C, Paulissen C, Baudelet E, Plaindoux E, Achouri Y, Calonne E et al. 2022. Mesp1 controls the chromatin and enhancer landscapes essential for spatiotemporal patterning of early cardiovascular progenitors. *Nat Cell Biol* **24**: 1114-1128.

Meilhac SM, Esner M, Kelly RG, Nicolas JF, Buckingham ME. 2004. The clonal origin of myocardial cells in different regions of the embryonic mouse heart. *Dev Cell* **6**: 685-698.

Mittnenzweig M, Mayshar Y, Cheng S, Ben-Yair R, Hadas R, Rais Y, Chomsky E, Reines N, Uzonyi A, Lumerman L et al. 2021. A single-embryo, single-cell time-resolved model for mouse gastrulation. *Cell* **184**: 2825-2842 e2822.

Nie J, Jiang M, Zhang X, Tang H, Jin H, Huang X, Yuan B, Zhang C, Lai JC, Nagamine Y et al. 2015. Post-transcriptional Regulation of Nkx2-5 by RHAU in Heart Development. *Cell Rep* **13**: 723-732.

Pan SJ, Tsang IW, Kwok JT, Yang Q. 2011. Domain adaptation via transfer component analysis. *IEEE Trans Neural Netw* **22**: 199-210.

Parameswaran M, Tam PP. 1995. Regionalisation of cell fate and morphogenetic movement of the mesoderm during mouse gastrulation. *Dev Genet* **17**: 16-28.

Peng G, Suo S, Cui G, Yu F, Wang R, Chen J, Chen S, Liu Z, Chen G, Qian Y et al. 2019. Molecular architecture of lineage allocation and tissue organization in early mouse embryo. *Nature* **572**: 528-532.

Peng H, Bria A, Zhou Z, Iannello G, Long F. 2014. Extensible visualization and analysis for multidimensional images using Vaa3D. *Nat Protoc* **9**: 193-208.

Pijuan-Sala B, Griffiths JA, Guibentif C, Hiscock TW, Jawaid W, Calero-Nieto FJ, Mulas C, Ibarra-Soria X, Tyser RCV, Ho DLL et al. 2019. A single-cell molecular map of mouse gastrulation and early organogenesis. *Nature* **566**: 490-495.

Qiu C, Cao J, Martin BK, Li T, Welsh IC, Srivatsan S, Huang X, Calderon D, Noble WS, Disteche CM et al. 2022. Systematic reconstruction of cellular trajectories across mouse embryogenesis. *Nat Genet* **54**: 328-341.

Ramirez F, Ryan DP, Gruning B, Bhardwaj V, Kilpert F, Richter AS, Heyne S, Dundar F, Manke T. 2016. deepTools2: a next generation web server for deep-sequencing data analysis. *Nucleic Acids Res* **44**: W160-165.

Riley P, Anson-Cartwright L, Cross JC. 1998. The Hand1 bHLH transcription factor is essential for placentation and cardiac morphogenesis. *Nat Genet* **18**: 271-275.

Saga Y, Miyagawa-Tomita S, Takagi A, Kitajima S, Miyazaki J, Inoue T. 1999. MesP1 is expressed in the heart precursor cells and required for the formation of a single heart tube. *Development* **126**: 3437-3447.

Sampath Kumar A, Tian L, Bolondi A, Hernandez AA, Stickels R, Kretzmer H, Murray E, Wittler L, Walther M, Barakat G et al. 2023. Spatiotemporal transcriptomic maps of whole mouse embryos at the onset of organogenesis. *Nat Genet* **55**: 1176-1185.

Schep AN, Wu B, Buenrostro JD, Greenleaf WJ. 2017. chromVAR: inferring transcription-factor-associated accessibility from single-cell epigenomic data. *Nat Methods* **14**: 975-978.

Schiebinger G, Shu J, Tabaka M, Cleary B, Subramanian V, Solomon A, Gould J, Liu S, Lin S, Berube P et al. 2019. Optimal-Transport Analysis of Single-Cell Gene Expression Identifies Developmental Trajectories in Reprogramming. *Cell* **176**: 928-943 e922.

Stringer C, Wang T, Michaelos M, Pachitariu M. 2021. Cellpose: a generalist algorithm for cellular segmentation. *Nat Methods* **18**: 100-106.

Trapnell C, Cacchiarelli D, Grimsby J, Pokharel P, Li S, Morse M, Lennon NJ, Livak KJ, Mikkelsen TS, Rinn JL. 2014. The dynamics and regulators of cell fate decisions are revealed by pseudotemporal ordering of single cells. *Nat Biotechnol* **32**: 381-386.

Tyser RCV, Ibarra-Soria X, McDole K, Arcot Jayaram S, Godwin J, van den Brand TAH, Miranda AMA, Scialdone A, Keller PJ, Marioni JC et al. 2021. Characterization of a common progenitor pool of the epicardium and myocardium. *Science* **371**.

Wamstad JA, Alexander JM, Truty RM, Shrikumar A, Li F, Eilertson KE, Ding H, Wylie JN, Pico AR, Capra JA et al. 2012. Dynamic and coordinated epigenetic regulation of developmental transitions in the cardiac lineage. *Cell* **151**: 206-220.

Wu T, Hu E, Xu S, Chen M, Guo P, Dai Z, Feng T, Zhou L, Tang W, Zhan L et al. 2021. clusterProfiler 4.0: A universal enrichment tool for interpreting omics data. *Innovation (Camb)* **2**: 100141.

Yang X, Hu B, Liao J, Qiao Y, Chen Y, Qian Y, Feng S, Yu F, Dong J, Hou Y et al. 2019. Distinct enhancer signatures in the mouse gastrula delineate progressive cell fate continuum during embryo development. *Cell Res* **29**: 911-926.

Zhang Q, Carlin D, Zhu F, Cattaneo P, Ideker T, Evans SM, Bloomekatz J, Chi NC. 2021. Unveiling Complexity and Multipotentiality of Early Heart Fields. *Circ Res* **129**: 474-487.

Zhang Y, Liu T, Meyer CA, Eeckhoute J, Johnson DS, Bernstein BE, Nusbaum C, Myers RM, Brown M, Li W et al. 2008. Model-based analysis of ChIP-Seq (MACS). *Genome Biol* **9**: R137.

Zheng M, Erhardt S, Ai D, Wang J. 2021. Bmp Signaling Regulates Hand1 in a Dose-Dependent Manner during Heart Development. *Int J Mol Sci* **22**.

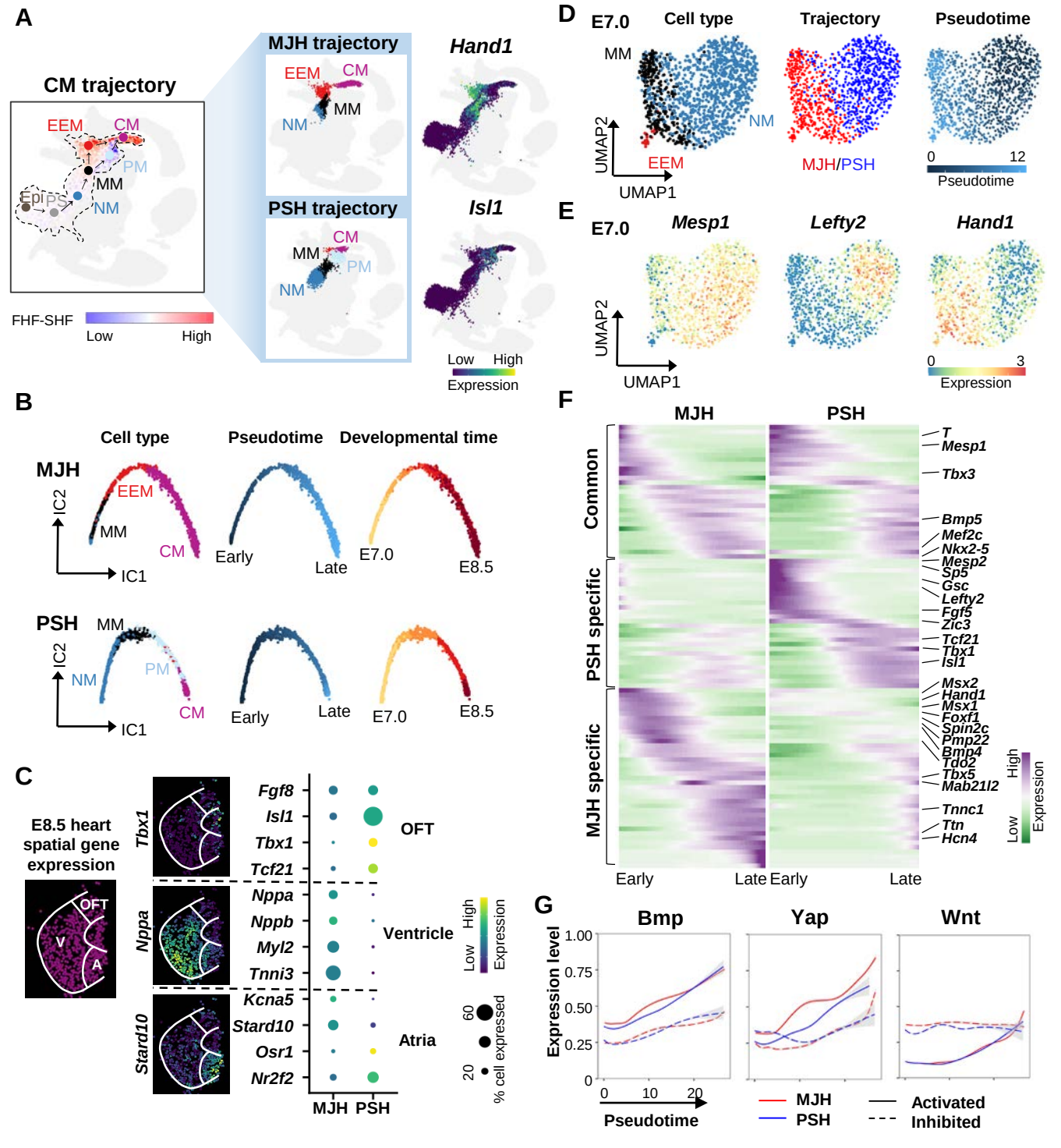
A
CM trajectory
EEM
CM
PM
MM
Epi
PS
NM
FHF-SHF
Low
High
MJH trajectory
EEM
CM
MM
NM
PSH trajectory
CM
MM
PM
NM
Hand1
Isl1
Low
High
Expression
B
Cell type
Pseudotime
Developmental time
MJH
IC2
IC1
EEM
MM
CM
Early
Late
E7.0
E8.5
PSH
MM
PM
NM
CM
C
E8.5 heart spatial gene expression
OFT
V
A
Tbx1
Nppa
Stard10
Fgf8
Isl1
Tbx1
Tcf21
Nppa
Nppb
Myl2
Tnni3
Kcna5
Stard10
Osr1
Nr2f2
OFT
Ventricle
Atria
MJH
PSH
High
Low
Expression
60
20
% cell expressed
D
E7.0
Cell type
Trajectory
Pseudotime
MM
NM
EEM
UMAP2
UMAP1
MJH/PSH
0
12
Pseudotime
E
E7.0
Mesp1
Lefty2
Hand1
UMAP2
UMAP1
0
3
Expression
F
MJH
PSH
Common
PSH specific
MJH specific
T
Mesp1
Tbx3
Bmp5
Mef2c
Nkx2-5
Mesp2
Sp5
Gsc
Lefty2
Fgf5
Zic3
Tcf21
Tbx1
Isl1
Msx2
Hand1
Msx1
Foxf1
Spin2c
Pmp22
Bmp4
Tdo2
Tbx5
Mab21l2
Tnnc1
Ttn
Hcn4
Early
Late
Early
Late
High
Low
Expression
G
Bmp
Yap
Wnt
Expression level
1.00
0.75
0.50
0.25
0
0
10
20
Pseudotime
MJH
PSH
Activated
Inhibited

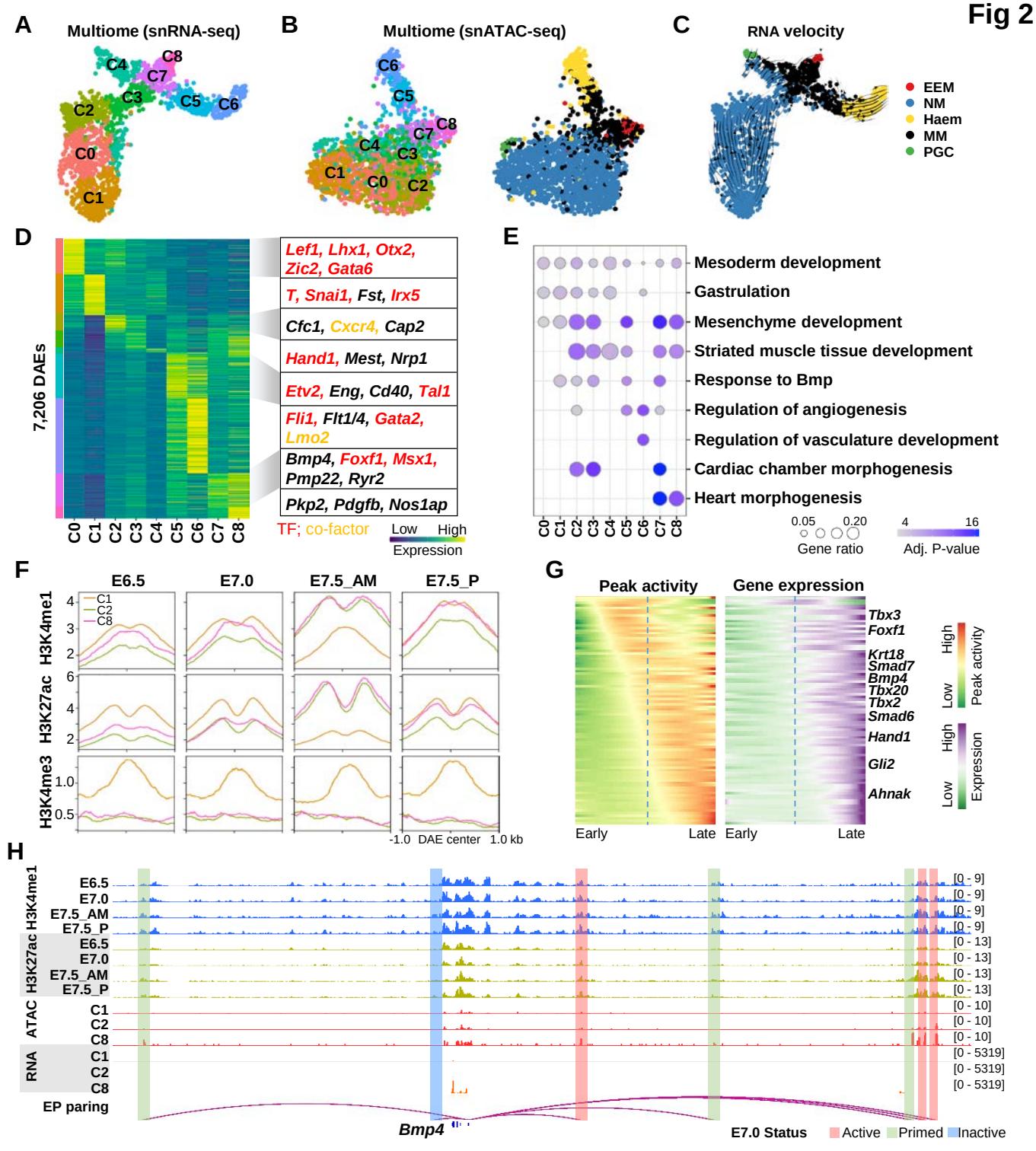
Fig 2
A
Multiome (snRNA-seq)
C4
C8
C7
C3
C5
C6
C2
C0
C1
B
Multiome (snATAC-seq)
C6
C5
C8
C7
C4
C3
C1
C0
C2
C
RNA velocity
EEM
NM
Haem
MM
PGC
D
7,206 DAEs
Lef1, Lhx1, Otx2, Zic2, Gata6
T, Snai1, Fst, Irx5
Cfc1, Cxcr4, Cap2
Hand1, Mest, Nrp1
Etv2, Eng, Cd40, Tal1
Fli1, Flt1/4, Gata2, Lmo2
Bmp4, Foxf1, Msx1, Pmp22, Ryr2
Pkp2, Pdgfb, Nos1ap
C0 C1 C2 C3 C4 C5 C6 C7 C8
TF; co-factor
Low High
Expression
E
Mesoderm development
Gastrulation
Mesenchyme development
Striated muscle tissue development
Response to Bmp
Regulation of angiogenesis
Regulation of vasculature development
Cardiac chamber morphogenesis
Heart morphogenesis
C0 C1 C2 C3 C4 C5 C6 C7 C8
0.05 0.20
Gene ratio
4 16
Adj. P-value
F
E6.5
E7.0
E7.5_AM
E7.5_P
H3K4me1
H3K27ac
H3K4me3
C1
C2
C8
-1.0 DAE center 1.0 kb
G
Peak activity
Gene expression
Tbx3
Foxf1
Krt18
Smad7
Bmp4
Tbx20
Tbx2
Smad6
Hand1
Gli2
Ahnak
Early Late Early Late
High Low Peak activity
High Low Expression
H
H3K4me1
E6.5
E7.0
E7.5_AM
E7.5_P
H3K27ac
ATAC
C1
C2
C8
RNA
EP paring
[0 - 9]
[0 - 13]
[0 - 10]
[0 - 5319]
Bmp4
E7.0 Status
Active
Primed
Inactive

A

MJH specific

Motif	P-value	Cand. TF
	1e-206	GATA4
	1e-62	TEAD4
	1e-41	FOXF1
	1e-28	HAND1

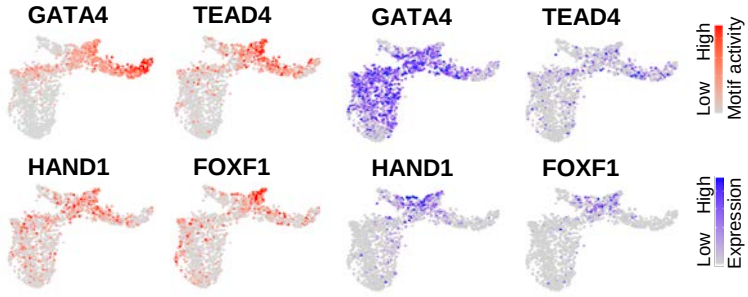

B

TEAD4
- Epithelium migration (2.1e-07)

HAND1 + TEAD4
- Cardiac chamber development (3.5e-13)

HAND1
- Negative regulation of growth (5.1e-05)
- Negative regulation of Wnt signaling pathway (1.7e-05)

HAND1 + FOXF1
- Cardiac chamber development (8.8e-07)

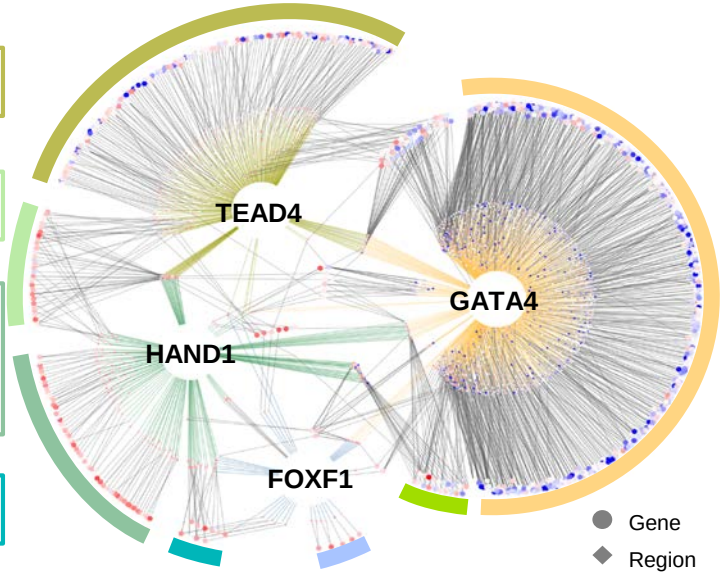

GATA4
- Gastrulation (2.7e-08)
- Maintenance of cell number (5.5e-08)
- Wnt signaling pathway (2.7e-08)

HAND1 + GATA4
- Mesenchyme development (4.4e-10)

FOXF1
- Response to Bmp (3.4e-03)

C

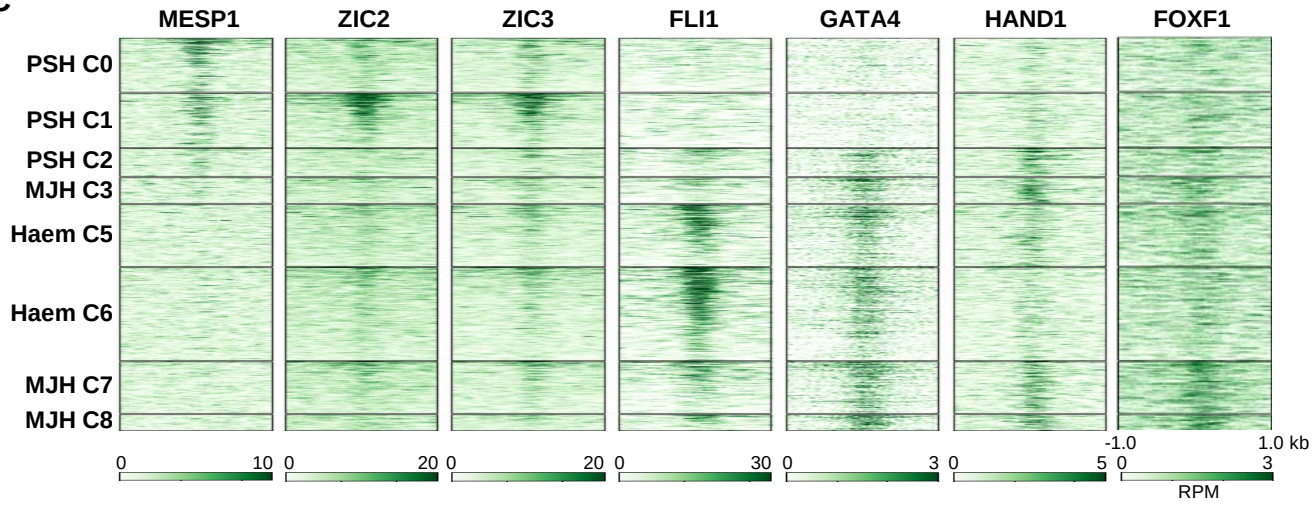

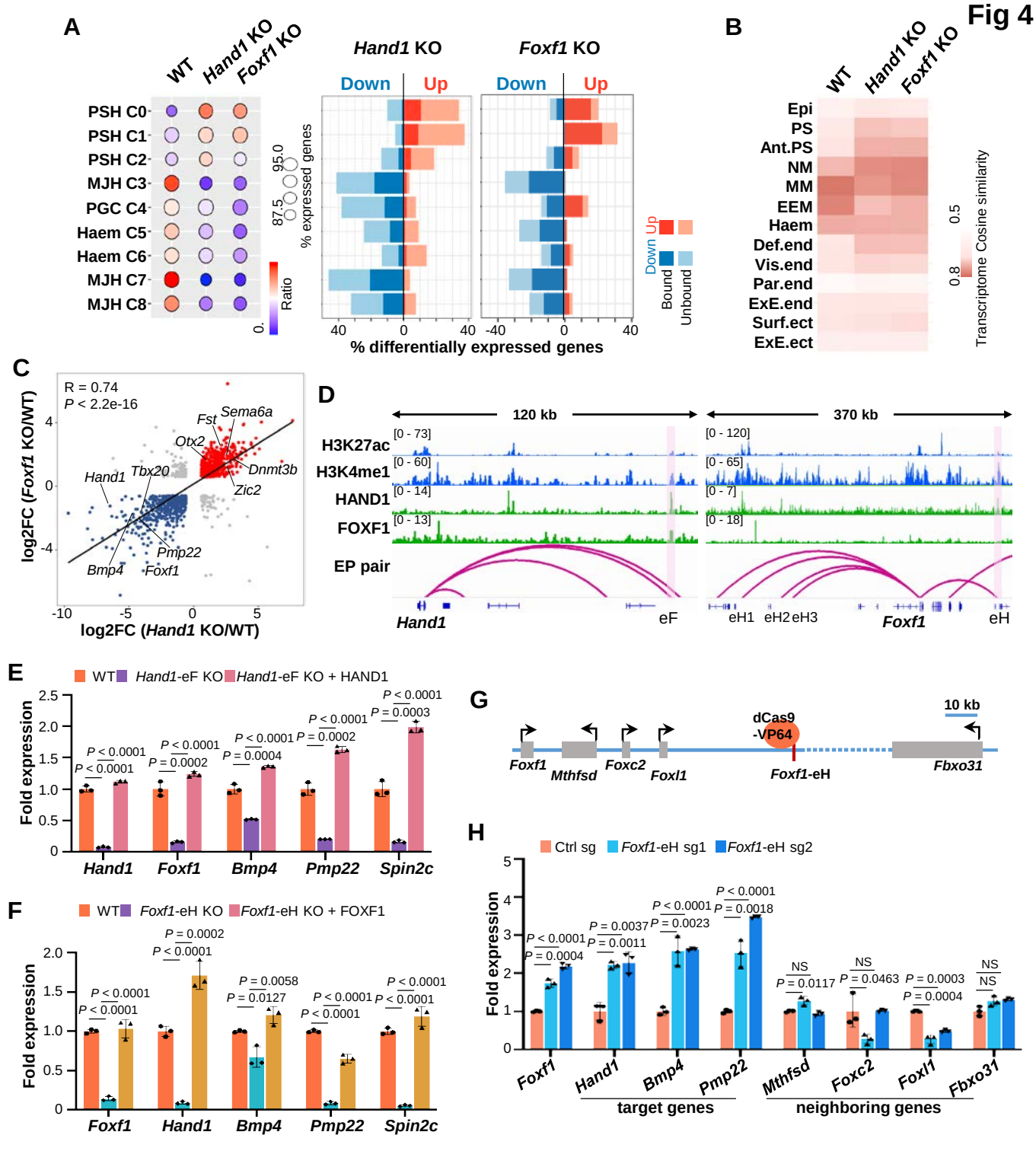
Fig 4
A
WT
Hand1 KO
Foxf1 KO
PSH C0
PSH C1
PSH C2
MJH C3
PGC C4
Haem C5
Haem C6
MJH C7
MJH C8
Ratio
% expressed genes
Hand1 KO
Foxf1 KO
Down
Up
% differentially expressed genes
Bound
Unbound
B
Epi
PS
Ant.PS
NM
MM
EEM
Haem
Def.end
Vis.end
Par.end
ExE.end
Surf.ect
ExE.ect
Transcriptome Cosine similarity
C
R = 0.74
P < 2.2e-16
Fst
Sema6a
Otx2
Dnmt3b
Zic2
Hand1
Tbx20
Pmp22
Bmp4
Foxf1
log2FC (Foxf1 KO/WT)
log2FC (Hand1 KO/WT)
D
120 kb
370 kb
H3K27ac
H3K4me1
HAND1
FOXF1
EP pair
Hand1
eF
eH1
eH2
eH3
Foxf1
eH
E
WT
Hand1-eF KO
Hand1-eF KO + HAND1
Fold expression
Hand1
Foxf1
Bmp4
Pmp22
Spin2c
F
WT
Foxf1-eH KO
Foxf1-eH KO + FOXF1
Fold expression
Foxf1
Hand1
Bmp4
Pmp22
Spin2c
G
10 kb
dCas9
-VP64
Foxf1
Mthfsd
Foxc2
Foxl1
Foxf1-eH
Fbxo31
H
Ctrl sg
Foxf1-eH sg1
Foxf1-eH sg2
Fold expression
Foxf1
Hand1
Bmp4
Pmp22
Mthfsd
Foxc2
Foxl1
Fbxo31
target genes
neighboring genes

Fig 5

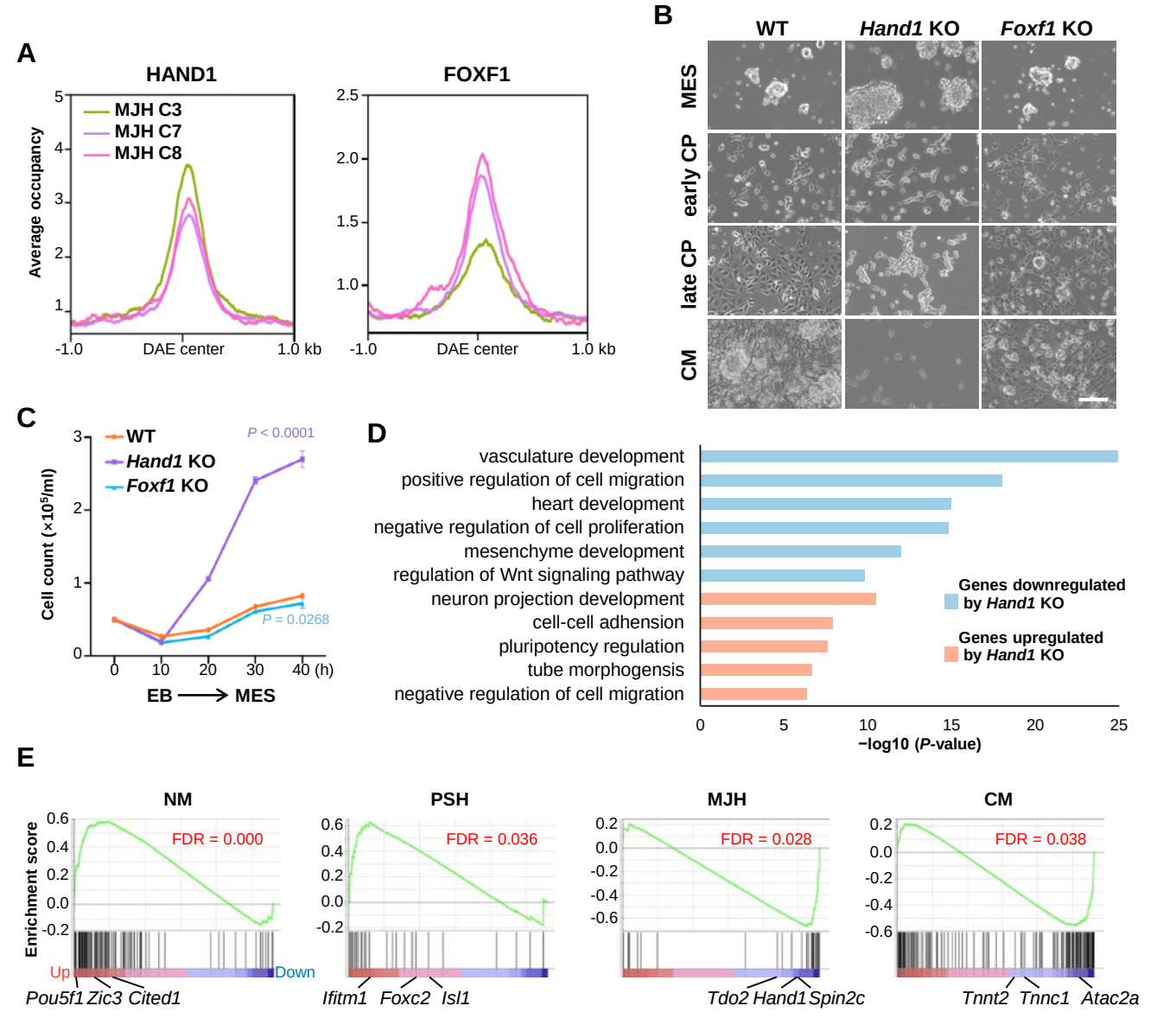
A
HAND1
FOXF1
MJH C3
MJH C7
MJH C8
Average occupancy
DAE center
1.0 kb
B
WT
Hand1 KO
Foxf1 KO
MES
early CP
late CP
CM
C
WT
Hand1 KO
Foxf1 KO
P < 0.0001
P = 0.0268
Cell count (×10⁵/ml)
EB → MES
D
vasculature development
positive regulation of cell migration
heart development
negative regulation of cell proliferation
mesenchyme development
regulation of Wnt signaling pathway
neuron projection development
cell-cell adhension
pluripotency regulation
tube morphogensis
negative regulation of cell migration
Genes downregulated by Hand1 KO
Genes upregulated by Hand1 KO
−log10 (P-value)
E
NM
PSH
MJH
CM
Enrichment score
FDR = 0.000
FDR = 0.036
FDR = 0.028
FDR = 0.038
Up
Down
Pou5f1 Zic3 Cited1
Ifitm1 Foxc2 Isl1
Tdo2 Hand1 Spin2c
Tnnt2 Tnnc1 Atac2a

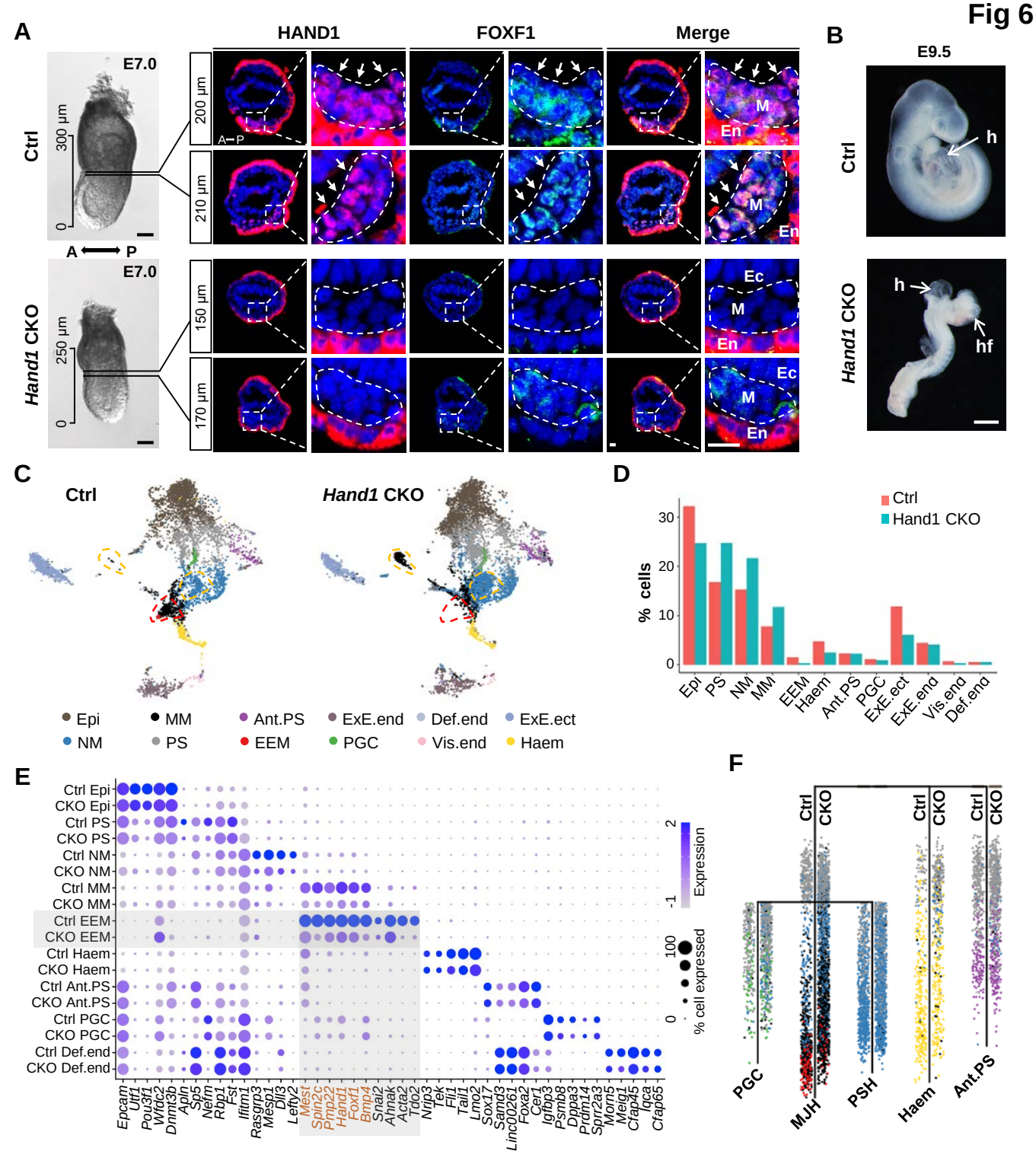
A
HAND1
FOXF1
Merge
Ctrl
E7.0
300 µm
0
200 µm
210 µm
A→P
M
En
A ⟷ P
Hand1 CKO
250 µm
150 µm
170 µm
Ec
B
E9.5
h
hf
C
Ctrl
Hand1 CKO
Epi
NM
MM
PS
Ant.PS
EEM
ExE.end
PGC
Def.end
Vis.end
ExE.ect
Haem
D
% cells
Ctrl
Hand1 CKO
Epi
PS
NM
MM
EEM
Haem
Ant.PS
PGC
ExE.ect
ExE.end
Vis.end
Def.end
E
Ctrl Epi
CKO Epi
Ctrl PS
CKO PS
Ctrl NM
CKO NM
Ctrl MM
CKO MM
Ctrl EEM
CKO EEM
Ctrl Haem
CKO Haem
Ctrl Ant.PS
CKO Ant.PS
Ctrl PGC
CKO PGC
Ctrl Def.end
CKO Def.end
Epcam
Utf1
Pou3f1
Wfdc2
Dnmt3b
Apln
Sp5
Nefm
Rbp1
Fst
Ifitm1
Rasgrp3
Mesp1
Dll3
Lefty2
Mest
Spin2c
Pmp22
Hand1
Foxl1
Bmp4
Snai2
Ahnak
Acta2
Tdo2
Ntrp3
Tek
Fli1
Tal1
Lmo2
Sox17
Sand3
Linc00261
Foxa2
Cer1
Igfbp3
Psmb8
Dppa3
Prdm14
Spnr2a3
Morn5
Melg1
Cfap45
Iqca
Cfap65
Expression
% cell expressed
F
Ctrl
CKO
PGC
MJH
PSH
Haem
Ant.PS

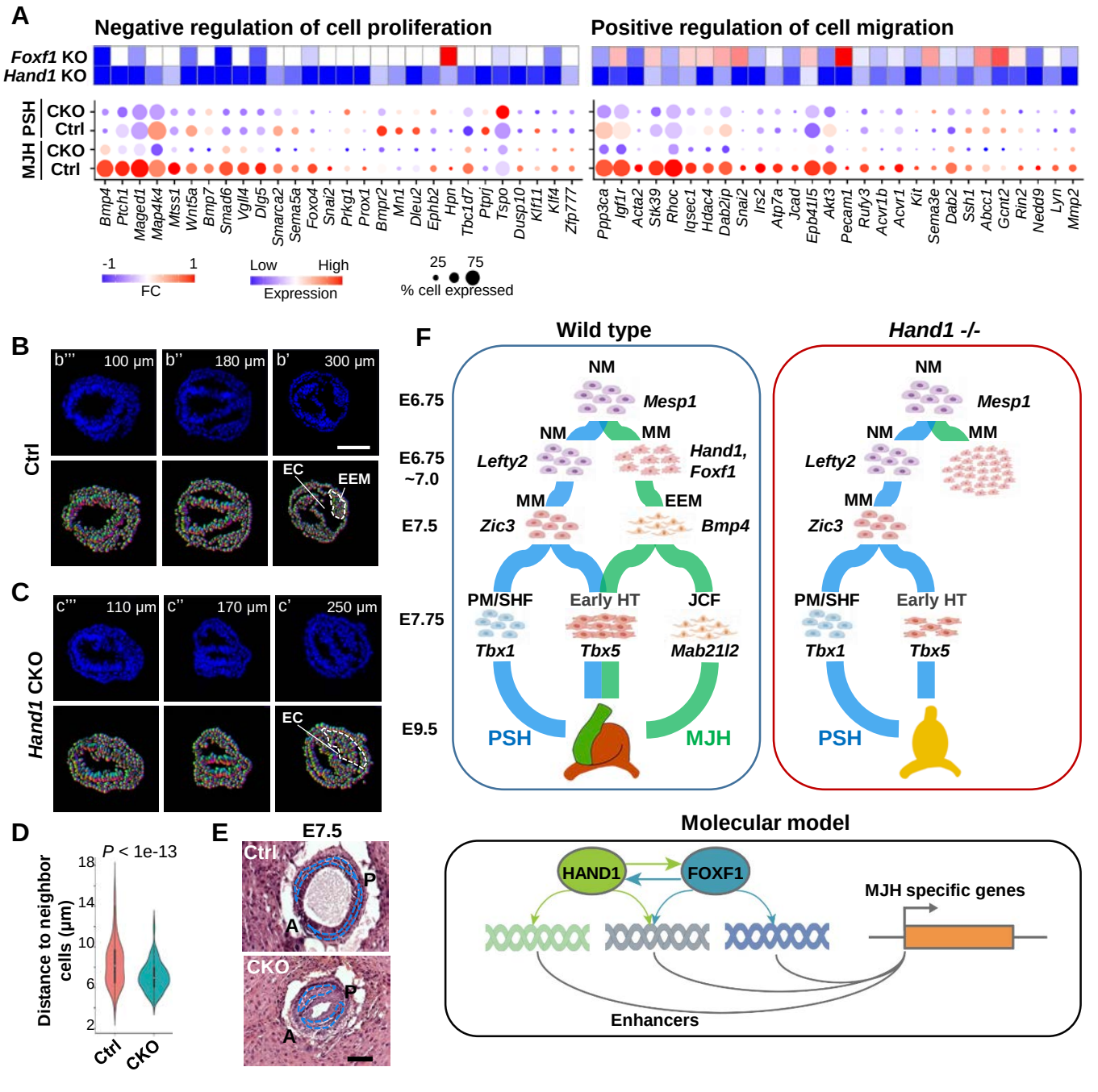
A
Negative regulation of cell proliferation
Positive regulation of cell migration
Foxf1 KO
Hand1 KO
PSH
MJH
CKO
Ctrl
Bmp4 Ptch1 Maged1 Map4k4 Mtss1 Wnt5a Bmp7 Smad6 Vgll4 Dlg5 Smarca2 Sema5a Foxo4 Snai2 Prkg1 Prox1 Bmpr2 Mn1 Dleu2 Ephb2 Hpn Tbc1d7 Ptprj Tspo Dusp10 Klf11 Klf4 Zfp777
Ppp3ca Igf1r Acta2 Stk39 Rhoc Iqsec1 Hdac4 Dab2ip Snai2 Irs2 Atp7a Jcad Epb41l5 Akt3 Pecam1 Rufy3 Acvr1b Acvr1 Kit Sema3e Dab2 Ssh1 Abcc1 Gcnt2 Rin2 Nedd9 Lyn Mmp2
-1
1
FC
Low
High
Expression
25
75
% cell expressed
B
b''' 100 μm
b'' 180 μm
b' 300 μm
Ctrl
EC
EEM
C
c''' 110 μm
c'' 170 μm
c' 250 μm
Hand1 CKO
EC
D
P < 1e-13
Distance to neighbor cells (μm)
18
14
10
6
2
Ctrl
CKO
E
E7.5
Ctrl
P
A
CKO
P
A
F
Wild type
Hand1 -/-
E6.75
E6.75 ~7.0
E7.5
E7.75
E9.5
NM
Mesp1
NM
MM
Lefty2
Hand1, Foxf1
MM
EEM
Zic3
Bmp4
PM/SHF
Early HT
JCF
Tbx1
Tbx5
Mab21l2
PSH
MJH
NM
Mesp1
NM
MM
Lefty2
MM
Zic3
PM/SHF
Early HT
Tbx1
Tbx5
PSH
Molecular model
HAND1
FOXF1
MJH specific genes
Enhancers

Fig. S1

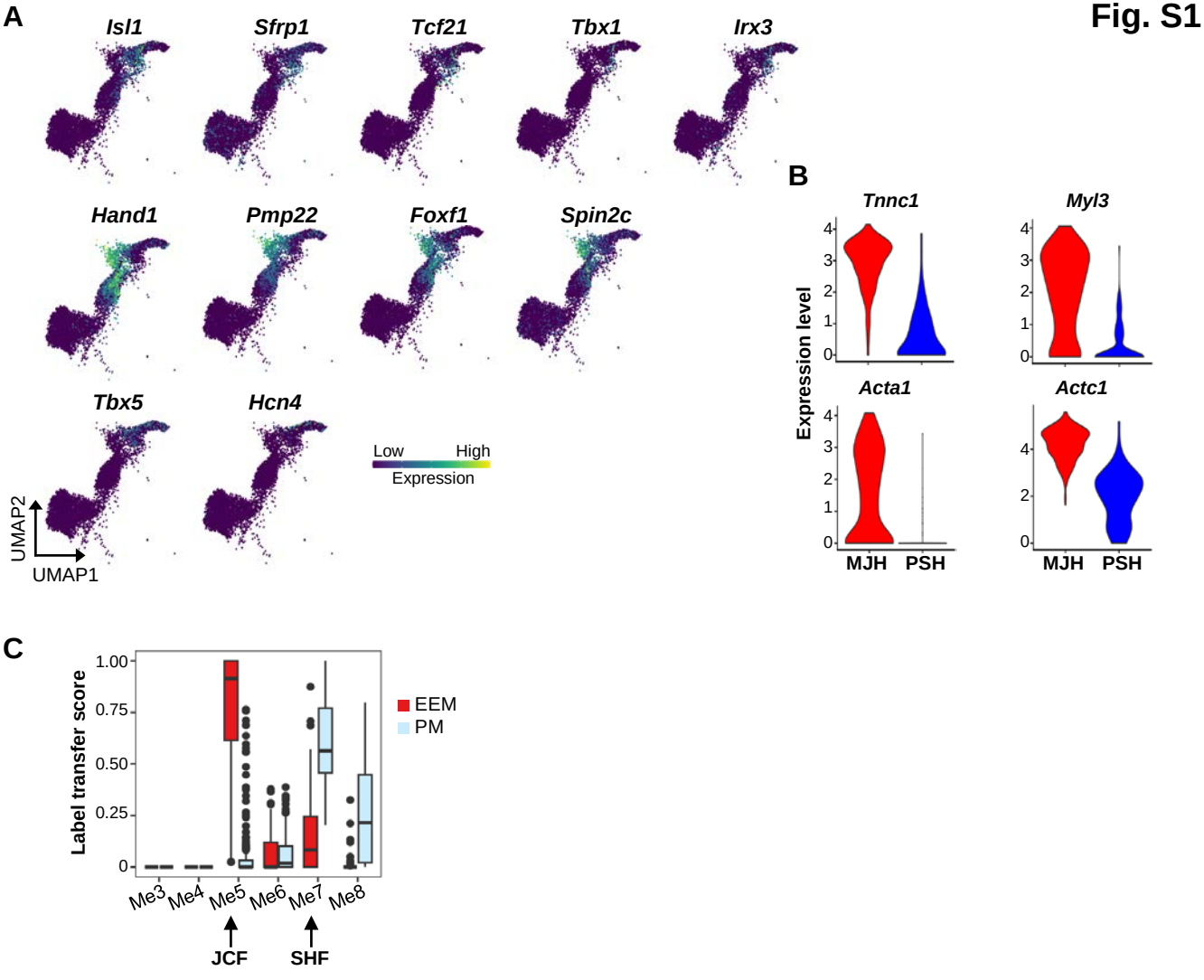
A
Isl1
Sfrp1
Tcf21
Tbx1
Irx3
Hand1
Pmp22
Foxf1
Spin2c
Tbx5
Hcn4
Low
High
Expression
UMAP2
UMAP1
B
Tnnc1
Myl3
Acta1
Actc1
Expression level
MJH
PSH
C
Label transfer score
1.00
0.75
0.50
0.25
0
EEM
PM
Me3
Me4
Me5
Me6
Me7
Me8
JCF
SHF

Fig. S2

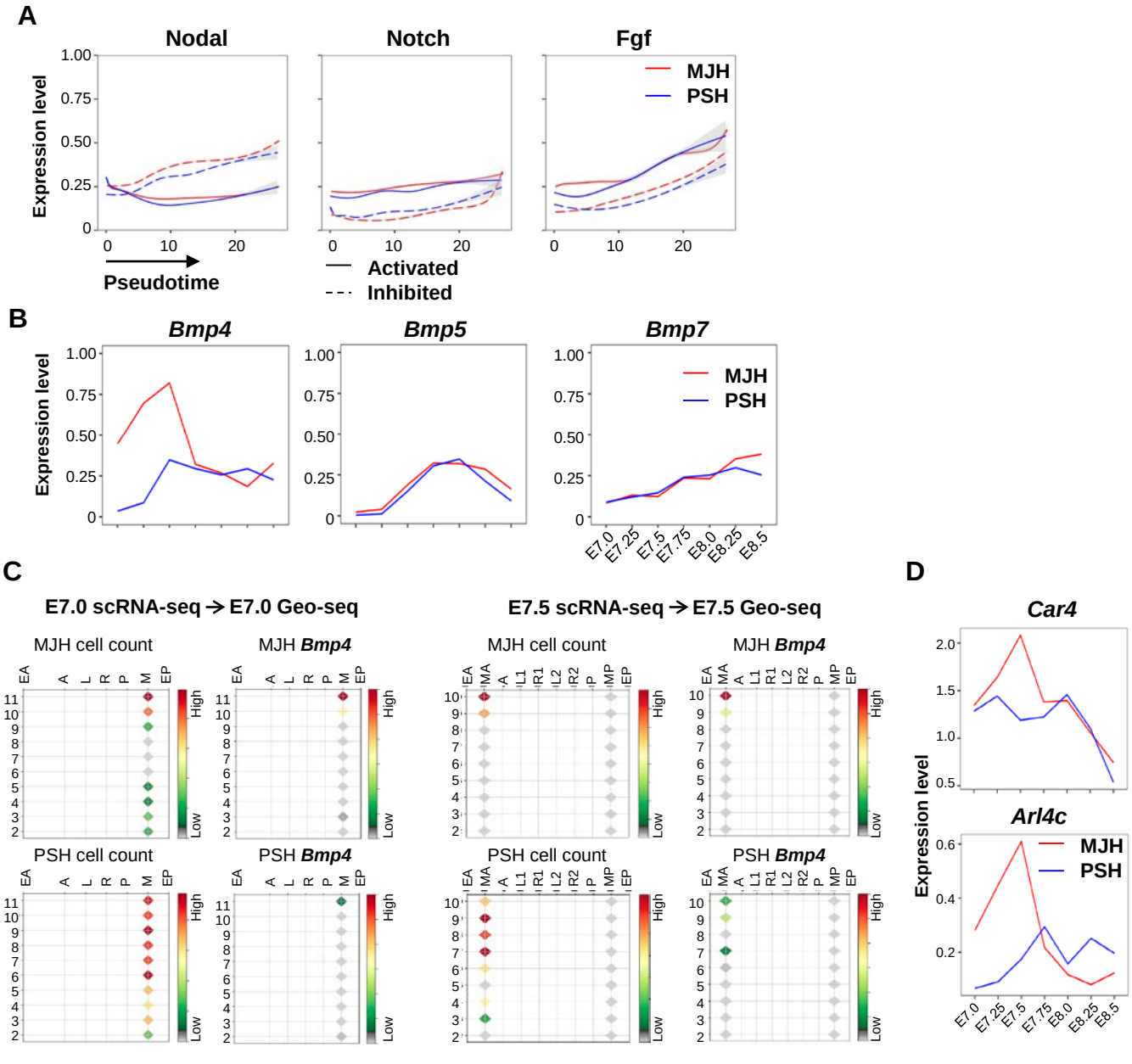
A
Nodal
Notch
Fgf
Expression level
1.00
0.75
0.50
0.25
0
0
10
20
Pseudotime
Activated
Inhibited
MJH
PSH
B
Bmp4
Bmp5
Bmp7
E7.0
E7.25
E7.5
E7.75
E8.0
E8.25
E8.5
C
E7.0 scRNA-seq → E7.0 Geo-seq
E7.5 scRNA-seq → E7.5 Geo-seq
MJH cell count
MJH Bmp4
PSH cell count
PSH Bmp4
EA
A
L
R
P
M
EP
MA
L1
L2
R1
R2
MP
High
Low
D
Car4
Arl4c

Fig. S3

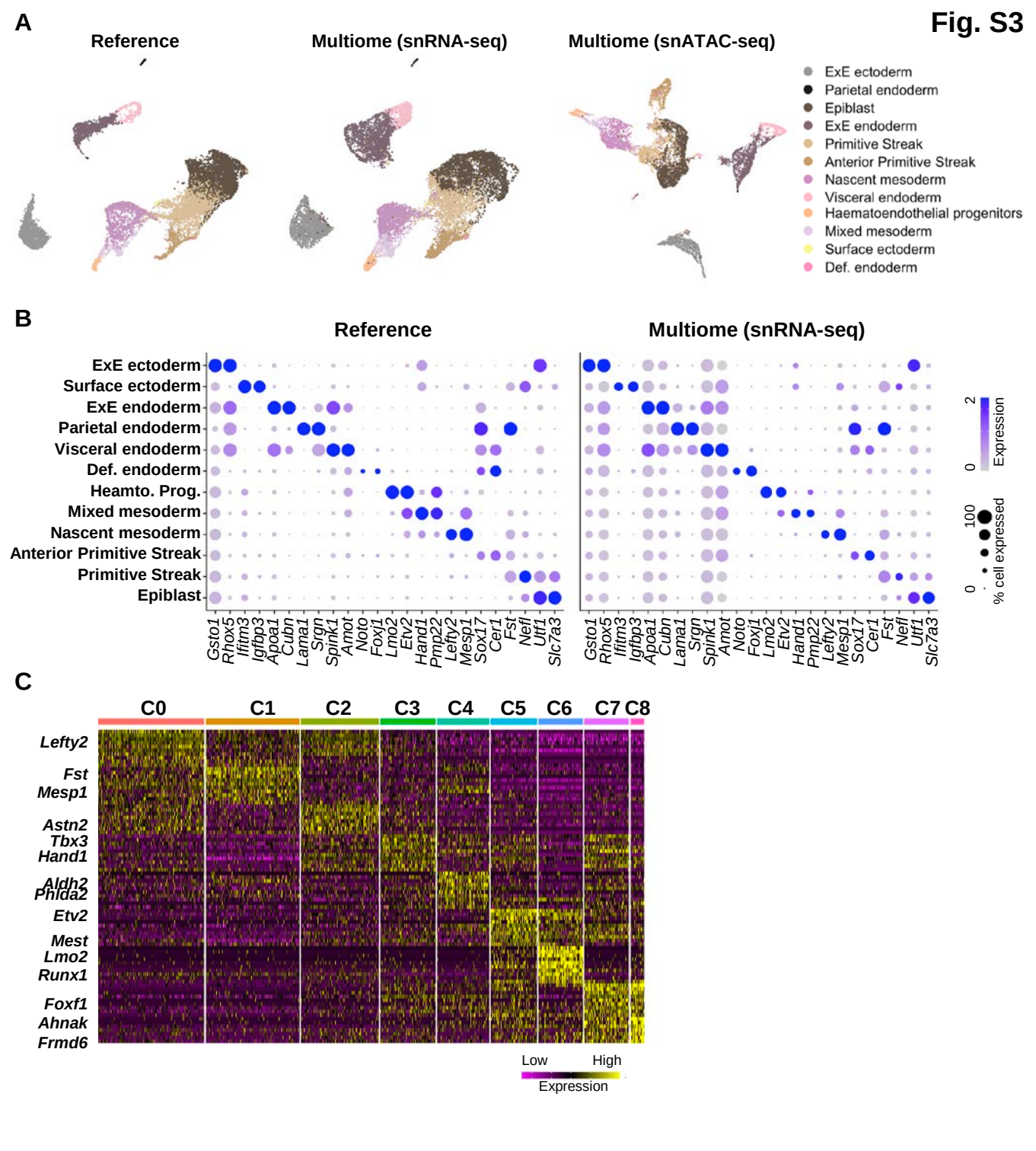
A
Reference
Multiome (snRNA-seq)
Multiome (snATAC-seq)
ExE ectoderm
Parietal endoderm
Epiblast
ExE endoderm
Primitive Streak
Anterior Primitive Streak
Nascent mesoderm
Visceral endoderm
Haematoendothelial progenitors
Mixed mesoderm
Surface ectoderm
Def. endoderm
B
Reference
Multiome (snRNA-seq)
ExE ectoderm
Surface ectoderm
ExE endoderm
Parietal endoderm
Visceral endoderm
Def. endoderm
Heamto. Prog.
Mixed mesoderm
Nascent mesoderm
Anterior Primitive Streak
Primitive Streak
Epiblast
Gsto1 Rhox5 Ifitm3 Igfbp3 Apoa1 Cubn Lama1 Srgn Spink1 Amot Noto Foxj1 Lmo2 Etv2 Hand1 Pmp22 Lefty2 Mesp1 Sox17 Cer1 Fst Nefl Utf1 Slc7a3
Expression
% cell expressed
C
C0 C1 C2 C3 C4 C5 C6 C7 C8
Lefty2
Fst
Mesp1
Astn2
Tbx3
Hand1
Aldh2
Phlda2
Etv2
Mest
Lmo2
Runx1
Foxf1
Ahnak
Frmd6
Low
High
Expression

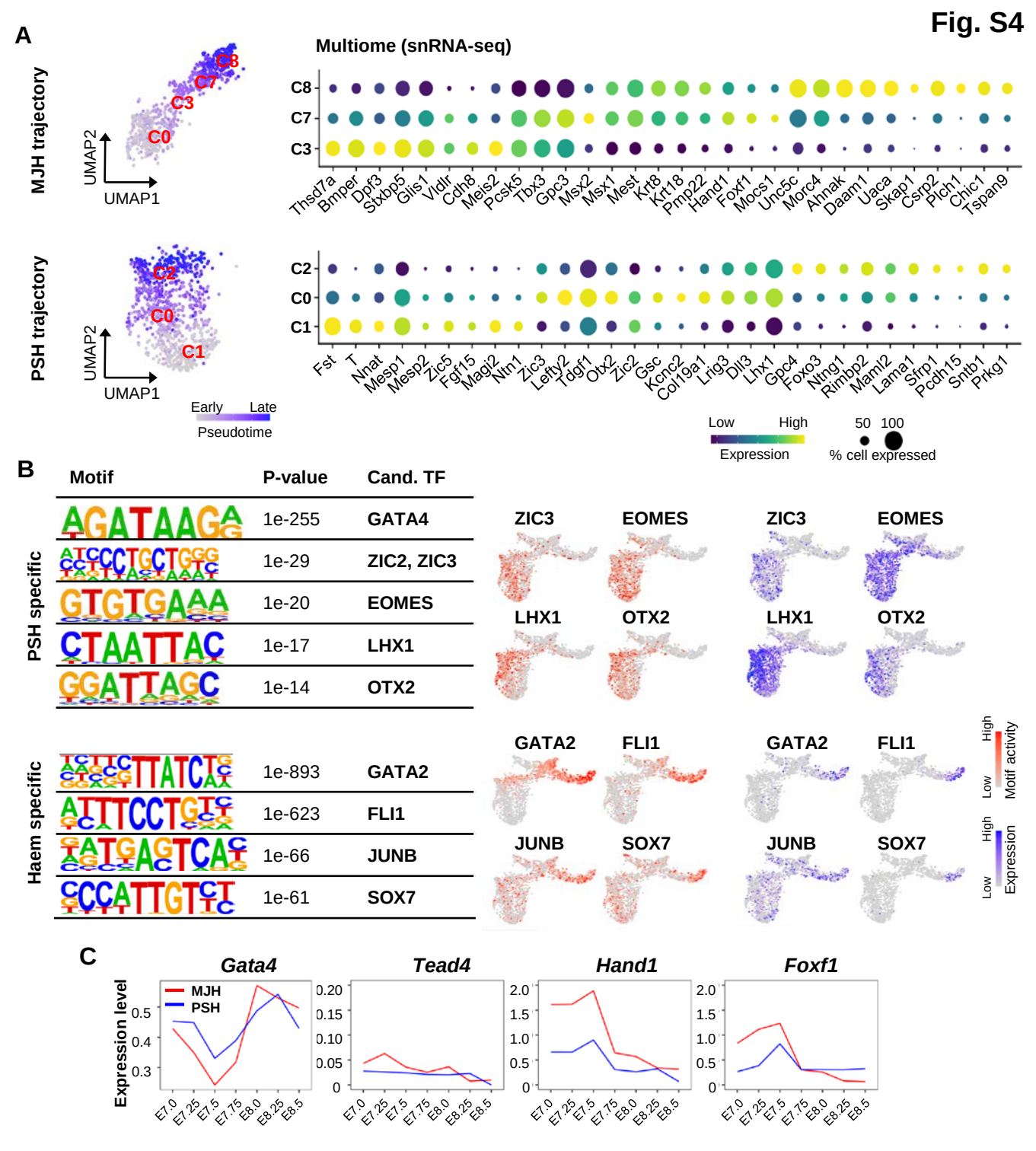
Fig. S4
A
Multiome (snRNA-seq)
MJH trajectory
C8
C7
C3
C0
UMAP2
UMAP1
Thsd7a Bmper Dpf3 Stxbp5 Glis1 Vldlr Cdh8 Meis2 Pcsk5 Tbx3 Gpc3 Msx2 Msx1 Mest Krt8 Krt18 Pmp22 Hand1 Foxf1 Mocs1 Unc5c Morc4 Ahnak Daam1 Uaca Skap1 Csrp2 Plch1 Chic1 Tspan9
PSH trajectory
C2
C0
C1
Fst T Nnat Mesp1 Mesp2 Zic5 Fgf15 Magi2 Ntn1 Zic3 Lefty2 Tdgf1 Otx2 Zic2 Gsc Kcnc2 Col19a1 Lrig3 Dll3 Lhx1 Gpc4 Foxo3 Ntng1 Rimbp2 Maml2 Lama1 Sfrp1 Pcdh15 Sntb1 Prkg1
Early Late
Pseudotime
Low High
Expression
50 100
% cell expressed
B
Motif
P-value
Cand. TF
PSH specific
1e-255 GATA4
1e-29 ZIC2, ZIC3
1e-20 EOMES
1e-17 LHX1
1e-14 OTX2
Haem specific
1e-893 GATA2
1e-623 FLI1
1e-66 JUNB
1e-61 SOX7
ZIC3 EOMES ZIC3 EOMES
LHX1 OTX2 LHX1 OTX2
GATA2 FLI1 GATA2 FLI1
JUNB SOX7 JUNB SOX7
High Low Motif activity
High Low Expression
C
Gata4
Tead4
Hand1
Foxf1
MJH
PSH
Expression level
E7.0 E7.25 E7.5 E7.75 E8.0 E8.25 E8.5

Fig. S5

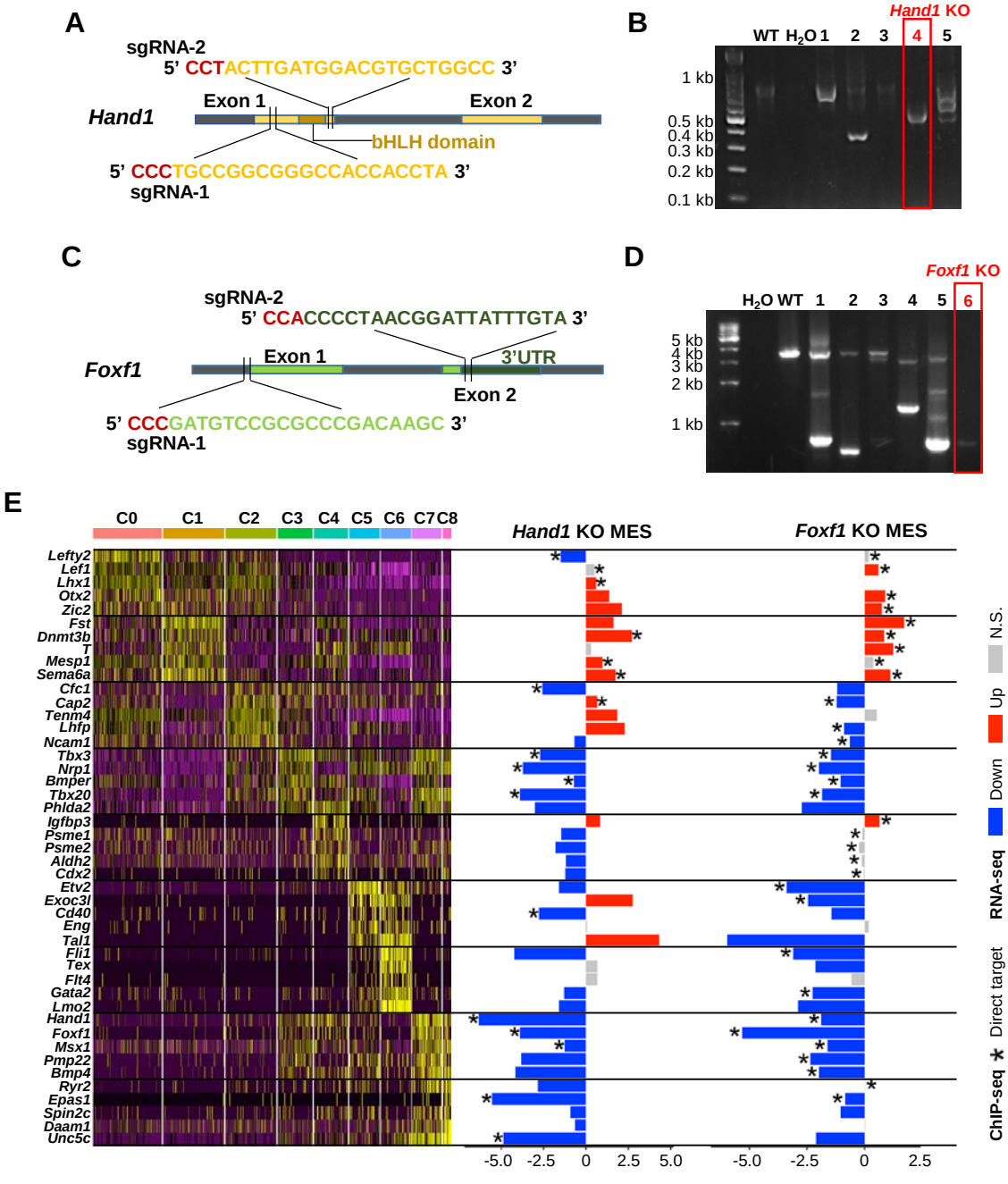
A
sgRNA-2
5' CCTACTTGATGGACGTGCTGGCC 3'
Hand1
Exon 1
Exon 2
bHLH domain
5' CCCTGCCGGCGGGCCACCACCTA 3'
sgRNA-1
B
Hand1 KO
WT H2O 1 2 3 4 5
1 kb
0.5 kb
0.4 kb
0.3 kb
0.2 kb
0.1 kb
C
sgRNA-2
5' CCACCCCTAACGGATTATTTGTA 3'
Foxf1
Exon 1
3'UTR
Exon 2
5' CCCGATGTCCGCGCCCGACAAGC 3'
sgRNA-1
D
Foxf1 KO
H2O WT 1 2 3 4 5 6
5 kb
4 kb
3 kb
2 kb
1 kb
E
C0 C1 C2 C3 C4 C5 C6 C7 C8
Hand1 KO MES
Foxf1 KO MES
Lefty2
Lef1
Lhx1
Otx2
Zic2
Fst
Dnmt3b
T
Mesp1
Sema6a
Cfc1
Cap2
Tenm4
Lhfp
Ncam1
Tbx3
Nrp1
Bmper
Tbx20
Phlda2
Igfbp3
Psme1
Psme2
Aldh2
Cdx2
Etv2
Exoc3l
Cd40
Eng
Tal1
Fli1
Tex
Flt4
Gata2
Lmo2
Hand1
Foxf1
Msx1
Pmp22
Bmp4
Ryr2
Epas1
Spin2c
Daam1
Unc5c
-5.0 -2.5 0 2.5 5.0
-5.0 -2.5 0 2.5
N.S.
Up
Down
RNA-seq
Direct target
ChIP-seq *

Fig. S6

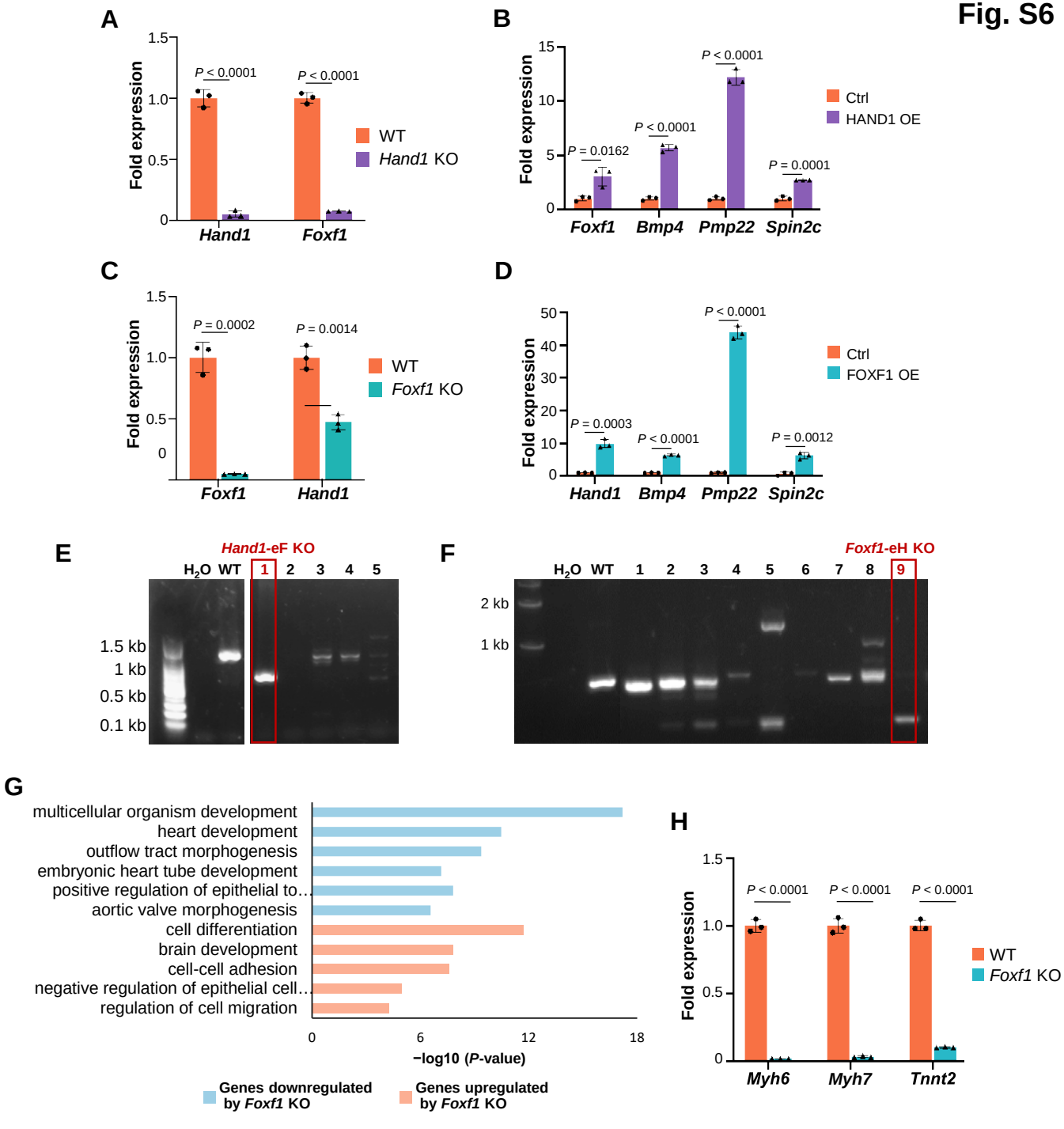
A
Fold expression
1.5
1.0
0.5
0
P < 0.0001
P < 0.0001
WT
Hand1 KO
Hand1
Foxf1
B
Fold expression
15
10
5
0
P = 0.0162
P < 0.0001
P < 0.0001
P = 0.0001
Ctrl
HAND1 OE
Foxf1
Bmp4
Pmp22
Spin2c
C
Fold expression
1.5
1.0
0.5
0
P = 0.0002
P = 0.0014
WT
Foxf1 KO
Foxf1
Hand1
D
Fold expression
50
40
30
20
10
0
P = 0.0003
P < 0.0001
P < 0.0001
P = 0.0012
Ctrl
FOXF1 OE
Hand1
Bmp4
Pmp22
Spin2c
E
Hand1-eF KO
H2O WT 1 2 3 4 5
1.5 kb
1 kb
0.5 kb
0.1 kb
F
Foxf1-eH KO
H2O WT 1 2 3 4 5 6 7 8 9
2 kb
1 kb
G
multicellular organism development
heart development
outflow tract morphogenesis
embryonic heart tube development
positive regulation of epithelial to…
aortic valve morphogenesis
cell differentiation
brain development
cell-cell adhesion
negative regulation of epithelial cell…
regulation of cell migration
0
6
12
18
−log10 (P-value)
Genes downregulated by Foxf1 KO
Genes upregulated by Foxf1 KO
H
Fold expression
1.5
1.0
0.5
0
P < 0.0001
P < 0.0001
P < 0.0001
WT
Foxf1 KO
Myh6
Myh7
Tnnt2

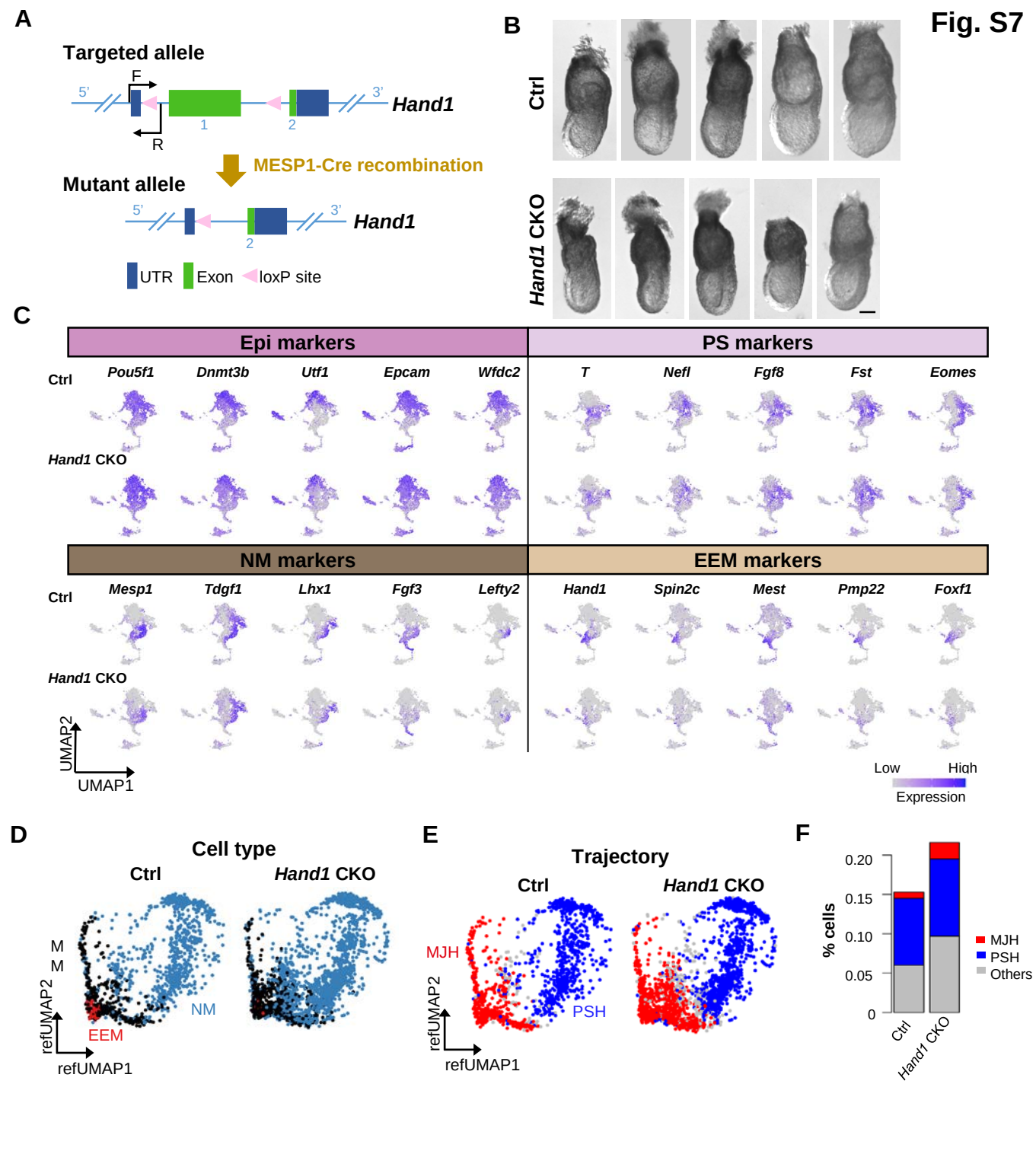
Fig. S7
A
Targeted allele
F
R
5'
3'
1
2
Hand1
MESP1-Cre recombination
Mutant allele
UTR
Exon
loxP site
B
Ctrl
Hand1 CKO
C
Epi markers
PS markers
NM markers
EEM markers
Pou5f1
Dnmt3b
Utf1
Epcam
Wfdc2
T
Nefl
Fgf8
Fst
Eomes
Mesp1
Tdgf1
Lhx1
Fgf3
Lefty2
Hand1
Spin2c
Mest
Pmp22
Foxf1
UMAP2
UMAP1
Low
High
Expression
D
Cell type
Ctrl
Hand1 CKO
M
M
NM
EEM
refUMAP2
refUMAP1
E
Trajectory
MJH
PSH
F
% cells
0.20
0.15
0.10
0.05
0
MJH
PSH
Others